ADDIS ABABA UNIVERSITY

COLLEGE OF NATURAL AND COMPUTATIONAL SCIENCES

MATERIALS SCIENCE PROGRAM UNIT

FIRST-PRINCIPLE STUDY OF VANDER WAALS HETERO-STRUCTURES OF $Graphene/MB_2$ (M = Fe, Mo) IN RECHARGEABLE LITHIUM-ION BATTERIES

By

Liya Gebrehiwot Gebremedhin

Masters Thesis

April 3 2024

Addis Ababa, Ethiopia

ADDIS ABABA UNIVERSITY
COLLEGE OF NATURAL AND COMPUTATIONAL SCIENCES
MATERIALS SCIENCE PROGRAM UNIT

FIRST-PRINCIPLE STUDY OF VANDER WAALS HETERO-STRUCTURES OF $Graphene/MB_2$ (M = Fe, Mo) IN RECHARGEABLE LITHIUM-ION BATTERIES

by

Liya Gebrehiwot Gebremedhin

Masters Thesis

April 3 2024

Addis Ababa, Ethiopia

Approved by	Signatures	Date
Dr.Yedilfana Setarge Advisor		
Prof. Ahmed Mustefa External Examiner	_____	_____
Dr. Getachew Gizaw Internal Examiner	_____	_____
Dr. Girum Ayalneh Chairman	_____	_____
	_____	_____

DEDICATION

This thesis is devoted to individuals who value knowledge and strive for academic success. This work is a testament to my family's love and support, to my mentors' wisdom, and to my beloved brother Temesgen Gebrehiwot, who has accompanied me on this journey.

ACKNOWLEDGMENTS

First and foremost, I want to express my heartfelt thankfulness to God for providing me the courage and clarity of mind to persist during my research trip. I'd like to thank my adviser, Dr. Yedilfana Setarge, for his important counsel, patience, and continuous support during this project. His views and experience in Computational Density Functional Theory (DFT) computations have been useful. His guidance not only molded my study, but also expanded my intellectual pursuits, resulting in the effective completion of this thesis.

I sincerely thank Dr. Getachew Gizaw, Dr. Girum Ayalneh, and Dr. Gamachis Sakata for their helpful input and support. Their efforts aided my academic progress, and I am grateful for their guidance. In addition, I am grateful to Addis Abeba University for offering me the female scholarship. This scholarship has been a source of financial and emotional support, allowing me to concentrate on my studies with commitment. I'd also like to thank my family for their everlasting love and encouragement, which has been a continual source of strength. Their efforts have not gone unappreciated, and I am eternally thankful for their faith in my abilities.

Finally, I value the companionship and moral support of my pals, particularly Desalegn Nigatu. Their encouragement was important to my academic progress. I'd like to express my deepest gratitude to everyone who helped, directly or indirectly, with the successful completion of this thesis.

TABLE OF CONTENTS

LIST OF ABBREVIATION

- ASE = Atomic Simulation Environment
- CI-NEB = Climbing Image Nudged Elastic Band
- DFT = Density Functional Theory
- ESDs =Energy Storage Devices
- GGA = generalized gradient approximation
- GLLBSC = Gritsenko, Leeuwen, Lenthe, and Baerends Solid State
- GPAW = Grid-based Projector-Augmented Wave
- IEA = international Energy Agency
- LIBs = Lithium-ion batteries
- Li-SBs = Lithium-sulfur batteries
- NRR = Nitrogen reduction reduction
- HER = Hydrogen evolution reaction
- HSE06 = Heyd-Scuseria-Ernzerhof
- LABs = Lithium-air batteries
- MBene = Transitional metal Boride
- MIBs = Magnesium-Ion Batteries
- PDOS = Project Density Of States
- PAW = Projected augmented wave
- PBE = Perdew Burke Ernzerhof
- 2D = two-Dimensional

- SIC = self-interaction correlation
- SIBs = Sodium-ion batteries
- TDOS = Total Density Of States
- TMDs = Transition Metal Dichalcogenides
- VASP = Vienna Ab initio Simulation Package code

LIST OF UNITS

- eV = electrovolt
- K = Kelvin
- $mAhg^{-1}$ = milli ampere hour per gram
- V = Volt
- Wh/kg = Watt-hour per kilogram

LIST OF TABLES

LIST OF FIGURES

ABSTRACT

The development of innovative, high-performance electrode materials is critical to the evolution of next-generation energy storage technologies. Due to their plentiful supplies and non-toxic properties, B-based 2D materials have gained attention. Density functional theory computations are used to examine the electrochemical characteristics of a number of 2D-MBenes as potential anode materials for Li-ion batteries. Both theoretical and experimental results confirmed the exciting potential of MBene for energy storage applications. We present a variety of 2D-MBenes-based hetero-structures based on first-principles density functional theory.

Computed the material by using the Vienna Ab initio Simulation Package code (VASP) [13]. The exchange-correlation potential was described by Perdew-Burk-Ernzerhof (PBE) generalized gradient approximation (GGA) functional. The convergence criterion of electron energy and ionic force were adopted with 10^{-5} eV and 0.05 $eV/\mathring{A}$ respectively. Monkhorst-Pack k-point grid with $5 \times 5 \times 1$ (001) the surface of both graphene/MoB_2 and Graphene/FeB_2 s HS by reducing the lattice mismatch between the two layers to 2.16% and 1.16% respectively.

We investigated the electrochemical characteristics, including open circuit voltage (OCV) ranging from 0.2 to 3V and theoretical capacities of up to 1040.1 mAh/g of graphene/MB_2 (M = Fe). Due to B_2Fe/graphene (-3.154 eV) exhibits more negative Li adsorption energies that have excellent electronic and ionic conductivities. CI-NEB technique estimates of lithium ion mobility and diffusion rates demonstrate the efficiency of these materials. These findings are critical for the development of effective lithium intercalation batteries, emphasizing the importance of material composition and diffusion paths.

Keywords: B_2Mo/graphene, B_2Fe/graphene, DFT, Hetero-structure, MBene, and Li-ion

CHAPTER 1

INTRODUCTION

1.1 Background

The swift advancement of artificial intelligence in agriculture, industries, service sectors, and communication technology has led to a significant growing demand for energy. However, this has harmed the environment, which is a major contributor to global warming, climate change, and public health due to the increase in energy consumption from fossil fuels rather than using renewable resources (wind, solar power, bio-energy, geothermal power, and others) [14, 15]. According to the International Energy Agency (IEA), fossil fuels such as coal, oil, and natural gas have continued to supply 78% of the world's energy needs; [16] the remaining less than 30% are renewable energy sources. To reduce the impact of humans on the environment and achieve a sustainable, clean energy future [17].

Maximizing energy storage is a long-standing technical and scientific challenge with worldwide ramifications for humanity. The specifications were created for the use of rechargeable lithium batteries. Next-generation rechargeable batteries include lithium-sulfur batteries (Li-SBs) and lithium-air batteries. Developing these technologies for demanding applications like fast-charging electric vehicles and grid storage can increase high-rate charge and cycle lifespan while maintaining energy density. Electronic materials have a crucial role in determining attributes, necessitating the creation of novel 2D materials. These days, 2D materials are widely used in technology, and researchers leverage the advancement of atomic technologies like flying minuscule atoms and molecules or sticking thin layers of materials

together to make new devices capable of incredible feats such as atomic layer deposition [18] and molecular beam epitaxy [19]. The synthesis of multiple layered compounds has produced a large number of layered compounds, some of which have been proposed as anode materials for metal-ion batteries

The first example of a 2D electrode material for LIBs is graphene [20]. Since then, anode materials for lithium-ion batteries (LIBs) have been researched using innovative 2D materials such as MoS_2 [21], VS_2 [22], phosphorene [23, 24], borophene [25], silicene [26], borophane [27], boron phosphide [28], Mo_2C [29], Ti_3C_2 [30]. Recently, there has been a lot of attention on the topic of 2D transition metal carbides or nitrides (MXene), which function as electrode materials for ion batteries, particularly anode materials, and MBene, as shown below in Figure 2 [31]. They are easier to synthesize, have high specific capacities, good electrical conductivity, highly active surfaces, high rate performance, and good structure stability.

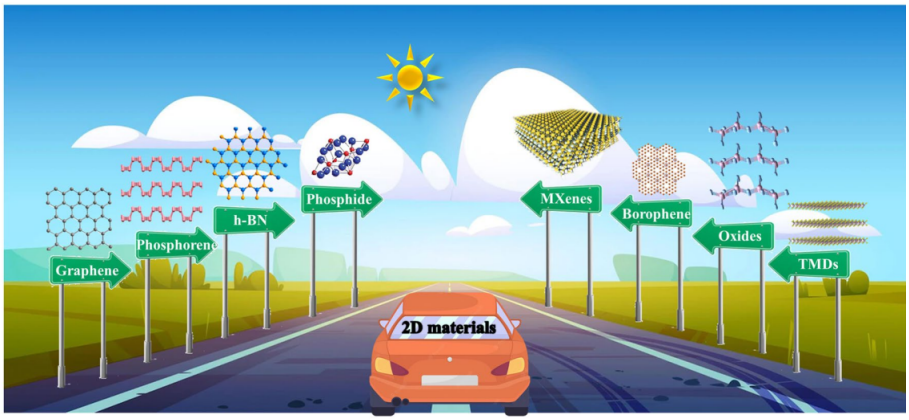

Figure 1: The rapid development of two-dimensional materials [1, 2]

The new family of 2D materials generated from the parent, $M_{n+1}B_n$ is as follows: "B" is for boron; and n = 1 to 4. "M" stands for early transition metals (Sc, Ti, Zr, Hf, V, Nb, Ta, Cr, or Mo) [7], which have even better possibilities for energy storage due to their highly conductive skeleton, high chemical activity, and quick charge carrier mobility [32]. Bano et al. (2018) [33] explored the driven metallic behavior and interfacial charge transport mechanism in MoS_2/MoB_2 heterostructures. Hetero-structures (HSs) are commonly used in

conventional semiconductors to create changeable electrical properties.

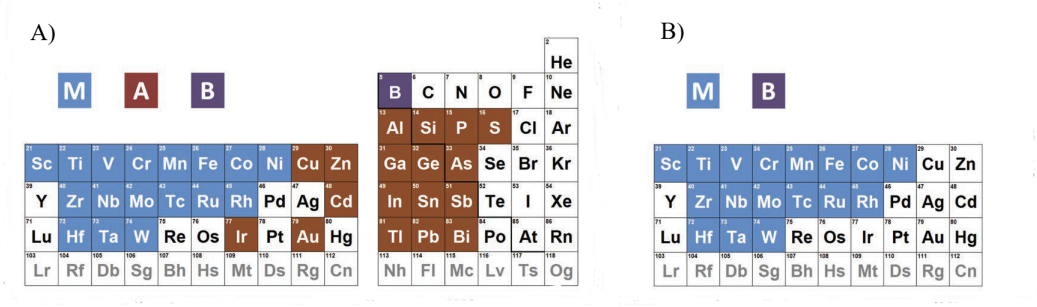

Figure 2: (A) MBene and (B) MAB phases [3]

The development of future two-dimensional materials has highlighted HSs with Van der Waals interactions as viable candidates. In 2019, Li et al. [34] demonstrated that the TiB monolayer has a higher potential as an anode material for Li/Na-ion batteries. Bhaskar et al. demonstrated in 2021 that Li may be stored between NiB layers and then deintercalated from the layered polymorphs of LiNiB molecules at room temperature. Wei et al. (2022) [35] used DFT simulations to predict that V_2B_2 would significantly adsorb Na ions, making it a suitable candidate for the anode material in sodium-ion batteries. Luo et al. [36] reported in 2023 that FeB_2 monolayers are high-capacity electrode materials for Mg-Ion batteries.

Researchers frequently estimate the structure, electrical properties, adsorption and diffusion properties of metal atoms on the MBene surface, open circuit voltage, and specific capacity of MBene to determine how effective it is as a material for metal ion battery electrodes [37]. Concerning the preceding debate, we have been inspired to investigate the electrical and thermoelectric characteristics of d graphene/MB_2 (M = Fe and Mo) HS theoretically. The reason we chose this particular mix of monolayers is that the boron-terminated MoB_2 and FeB_2 layers have a broad range of chemical potentials that can be tolerated by thermodynamics, which makes them intriguing from an electronic standpoint [38].

1.2 Statement of the problem

In order to address the growing need for energy storage and economics, the world of today demands incredibly efficient technology. Rechargeable metal-ion batteries have drawn a lot of attention as cutting-edge technologies for inexpensive renewable energy storage because of their plentiful supplies and environmentally favorable characteristics. In addition, because of their low price and high energy densities, rechargeable Li-ion batteries are thus gaining popularity. However, there are still issues such as volume instability, low voltage, and dendrite formation, just to mention a few, that need to be solved for the next-generation Li-ion batteries. In order to solve this problem, 2D materials for use as anode electrodes have recently attracted considerable attention to improving their electronic properties and electrochemical properties. MBenes such as MB_2 (M=Mo, Fe) are among the 2D materials that are specifically used for this purpose. Their properties are adaptable and can be customized for energy storage systems due to their excellent performance, which includes outstanding safety and rating skills. Herein we are interested in giving attention to graphene/MB_2 (graphene, M = Fe, Mo) as anode materials for rechargeable Li-ion batteries from first-principles studies.

1.3 Objective

1.3.1 General Objective

The main objective of this study is to investigate the first-principles study of graphene/MB_2 (M=Fe, Mo) and MB_2(M=Fe, Mo)/graphene Vander Waals hetero-structures as anode materials in rechargeable lithium-ion batteries.

1.3.2 Specific objective

The specific objectives of this study are:

- To investigate the structural and electronic properties of the structures of MB_2 (M = Fe, Mo), Graphene, and their hetero-structures, including the energy, crystal geometry information, density of states, and band structures.
- To determine the structural stability, such as formation energy as a function of interlayer distance of both pristine and hetero-structures.
- To examine the adsorption energies of Li on pristine and hetero-structures as well as the effect of Li-ion concentration on adsorption on hetero-structures.
- To estimate the average open-circuit voltage (OCV), theoretical storage capacity, and Li-ion diffusion studies in graphene /MB_2 and MB_2/graphene hetero-structures.

1.4 Scope and Limitations of Research

In this work, the electrical properties, hetero-structure thermodynamic stability, optimal positions for lithium (Li) atom adsorption, and energy storage capacity and NEB calculation of graphene/MB_2 (M = Fe, Mo) and MB_2/graphene hetero-structures for rechargeable lithium batteries are examined using Density Functional Theory (DFT). Since DFT-based computational modeling occupies much of the work, theoretical predictions rather than experimental validation are necessarily the study's only possible application..

The electrical characteristics of the structures are estimated using the Generalized Gradient

Approximation-Perdew, Burke, and Ernzerhof (GGA-PBE) method. The GGA-PBE approximation is well known for overstating electrical properties, though. In order to better define electrical features, the Heyd-Scuseria-Ernzerhof (HSE06) hybrid functional and the Gritsenko, Leeuwen, Lenthe, and Baerends Solid State (GLLBSC) potential are included in the solution.

Specifically, the HSE06 method works well with the d orbitals of transition metals. There are certain limitations to the research despite these methodological advancements. The optical and mechanical properties MBene-based heterostructures were not computed in this work due to computation cost. This points to a research hole that may be filled by subsequent investigations, contributing to a more comprehensive understanding of the behavior of these materials in real-world applications.

1.5 Significant Of The Study

For the energy storage industry as well as the scientific community, this work constitutes a major technological advance. This work explores the computational modeling of graphene/MB_2 (M = Fe, Mo) and MB_2 (M = Fe, Mo)/graphene MBene-based hetero-structures, laying a strong foundation for future research into anode materials for various types of rechargeable lithium batteries, including Lithium-ion Batteries (LIBs), Lithium-sulfur Batteries (Li-SBs), and Lithium-air Batteries (LABs).

We provide insights from our Density Functional Theory (DFT) research that will be the basis for upcoming computational and experimental endeavors. They provide a comprehensive understanding of these hetero-structures' structural integrity and electrochemical activity, which is necessary for developing and creating next-generation anode materials. These findings have a number of possible applications, one of which is as a guide for enhancing the effectiveness and performance of systems that use rechargeable lithium batteries.

Moreover, the market for energy storage could be completely changed by the study's con-

clusions. We might contribute to the development of batteries with greater capacity, longer life cycles, and improved safety profiles by directing the experimental design and synthesis of these novel materials. This research contributes to the global search for dependable and sustainable energy sources while also advancing the science of energy storage.

1.6 Organization of the Study

The five sections of this master's thesis are as follows. The introductory chapter sets the scene for the study, clarifies its goal, highlights important issues, and delineates its goals. It highlights the importance and contribution of the study.

The second section of the literature review is a critical synthesis of pertinent scholarly works that offers a thorough rundown of the state of the field's research at the moment. This chapter places the thesis in the context of the existing body of knowledge, emphasizing the ways in which it both builds upon and departs from previous studies. It also shows gaps in the literature that the current study aims to address, demonstrating the significance and applicability of the research.

The computational method (third chapter) The study's methodological framework, including techniques for collecting research data and analytical techniques, is covered in this chapter. It provides an open overview of the methods, guaranteeing the study's reliability and repeatability.

The results of the investigation are succinctly summarized in the fourth chapter, Results and Discussion. It looks at the results in relation to the research questions and previously reviewed literature. This chapter provides significant conclusions on the implications of the study in addition to summarizing and interpreting the data. The research findings are summarized in the final chapter, Recommendations, which also makes conclusions based on the available evidence.

CHAPTER 2

LITERATURE REVIEW

2.1 Lithium-ion Batteries

Among all anode materials because of its encouraging qualities. According to Whitingham (1976), the electrical potential of this material is the lowest ($-3.04, \mathrm{V}$ vs. SHE), and its theoretical capacity is the larges. But the lithium metal anode has problems with dendritic formation, low Coulombic efficiency, and cycle life[39]. To address these issues, many approaches have been put forth, including surface modification, electrolyte optimization, and host matrix design[40].

Due to their special qualities, such as their large surface area, rapid charge transfer, adjustable band gap, and flexibility, two-dimensional (2D) anode materials have been more and more well-liked in recent years [41, 42]. Numerous applications for 2D materials are anticipated, such as fuel cells, electrochemical processes, electrical devices, sensor applications, energy storage, catalysis, and renewable energy technologies. Because of their dimensions and size, these 2D materials have special properties [43].

Since graphene has a large theoretical capacity of $744, \mathrm{mAhg}^{-1}$, strong electric conductivity, and mechanical durability, it is the most studied 2D material for use as an anode material in Lithium-ion batteries[44, 45]. Nevertheless, challenges like severe aggregation, low lithium-ion diffusion coefficient, poor cycle life, large volume expansion, and lower capacity relative to lithium metal anodes [46, 47] limit its practical application.

MBenes' multi-layered structure, large specific surface area, and numerous active centers enhance the efficiency of lithium ion insertion and storage. The battery's efficiency varies depending on the characteristics of the lithium ions, even though MBene functions similarly for various lithium ions[48]. Theoretically, it has been demonstrated that MBenes are successful as anode materials for LIBs. Additionally, MBenes have a higher theoretical capacity than other two-dimensional materials, making them more beneficial as negative electrodes [49, 50].

2.2 The working principle of lithium-ion batteries

The better recharge and electrochemical cell utilization properties of lithium-ion batteries are well recognized.comprise a separator, a porous polymer membrane that permits lithium to flow while preventing short circuiting between the two electrodes, which are the anode and cathode, and an electrolyte. Their amazing capacity to both emit and absorb electrons and lithium ions alters their chemical composition significantly. These batteries have an intricate system that efficiently stores and distributes electrical energy. It is made possible by redox reactions involving electron exchange [51].

An essential part of the battery is the electrolyte, which facilitates the passage of lithium ions between the electrodes to produce an electric current that can power a variety of devices. Fast ionic charge transfer is made possible by the high concentration of Li-ions in the electrolyte, which improves cell operation. According to Thackeray (2012) and Glaize (2013), the electrolyte needs to be both electrically insulating and ionically conductive.The rocking chair principle applies to rechargeable batteries. During the discharge process, electrons are drawn from the graphite (negative electrode) and transferred to the outside circuit, where they are adsorbed onto the positive electrode ($LiCoO_2$ means cathode) (Figure.3).

A portion of the electrons are used by the device. After passing through the device and the circuit, electrons continue to flow to the cpositive electrode ($LiCoO_2$). To maintain

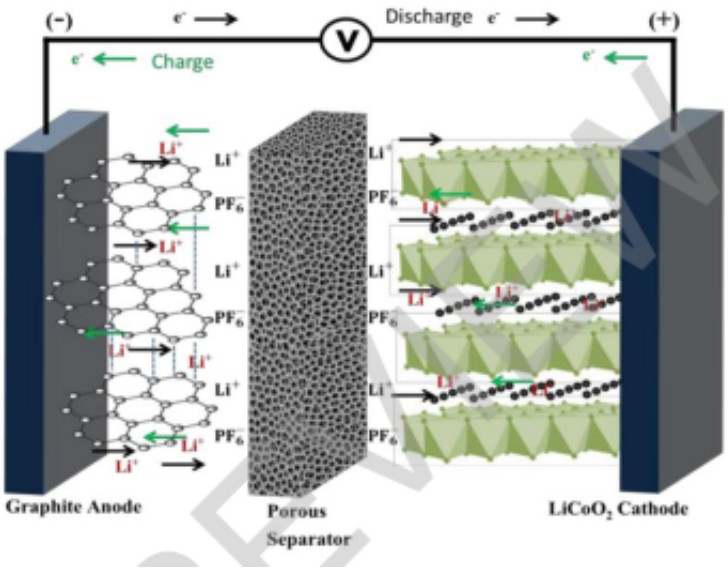

Figure 3: Schematic of the configuration of LIBs [4]

electrical neutrality in the positive electrode , lithium ions move back and forth between the electrodes. The electrical current that powers the electronic devices is created by electrons traveling across the external circuit. Reversible processes take place when Li moves from the positive electrode to the negative electrode and electrons move from the external circuit during the charging process via an external load (figure 3)[52, 53]. In addition, from the graphite anode to the $LiCoO_2$ cathode, lithium ions move within the cell [54]. The following is a summary of the electrochemical processes involved in the charge/discharge process [55].

$$\text{Anode: } 6\text{C} + x\text{Li}^+ + x\text{Li}^- \rightleftharpoons x\text{LiC}_6 \tag{1}$$

$$\text{Cathode: } \text{LiCoO}_2 \rightleftharpoons \text{Li}_{1-x}\text{CoO}_2 + xe^- \tag{2}$$

$$\text{Overall:} \text{LiCoO}_2 \rightleftharpoons x\text{LiC}_6 + \text{Li}_{1-x}\text{CoO}_2 \tag{3}$$

With their own layered architectures, intriguing alternatives like MBenes offer the possibility of even higher energy storage capacities. As scientific research progresses, batteries will

experience additional development to provide cleaner and more effective energy solutions, thereby contributing to a sustainable future.

2.3 Anode materials

The anode is one of the parts of the battery that stores energy. They have higher specific capacities than traditional graphite and potentially double the energy density of lithium-ion batteries (LIBs) [56]. In LIBs, new anode materials are becoming more and more popular. A range of components are included in these materials, such as silicon, metals, metal oxides, metal sulfides, lithium metal, and various carbons, according to reports. By Shuai Kang and Junjie Niu. [57] the creation of high-capacity anode materials to meet the expanding need for energy storage that is more efficient and sustainable.

2.3.1 Lithium Metal Anode

It is possible to employ metallic lithium as an anode material. In reality, the principal anode material for lithium-batteries was metallic Li. It have the lowest density , the lowest electro-chemical potential compared to other the [58]. Unlike graphite anodes, which use intercalation/deintercalation mechanisms, lithium-metal anodes use a conversion reaction between metallic Li and Li-ions.

The specific energy of lithium-ion batteries (LIBs) with Li-containing TMO as cathodes can rise from 280 to around 440 Wh/kg [59] once the anode is changed to Li metal. However, the practical applications of Li anodes are limited by uncontrolled growth of Li dendrites, which leads to a short lifespan and significant safety issues. To solve these issues, a few successful techniques have been used, such as membrane modification, the addition of protective layers, nanostructured anodes, and electrolyte modification. Because of its reactivity, Li metal requires a great deal more effort before it can be used in batteries, even though the experimental results are encouraging.

2.4 Introduction of MBene

The novel 2D material of MBene are built around the combining of boron and different transition metals. MBene derived (where "M" is the early transition metal and "B" is the boron element) [60]. MBenes were different derived (Au_2B, MnB, Nb_5B_2, HfB, ZrB, Mo_2B, Nb_3B_4, Ta_3B_4, OsB_2, RuB_2 and FeB_2), clarifying properties such as high mechanical and thermal stabilities and low fracture strength. To stabilize the boron sheet, the transition metal would give boron electrons[61]. It is commonly known that these materials' structure vary greatly (Figure 4). The multi-centered bonding of B, which results in a variety of metal-boride properties [5].A new dimension to the rich science of metal borides has been added in the last few years with the development and with superior thermal conductivity,and excellent electron conductivity are becoming more desirable [62].

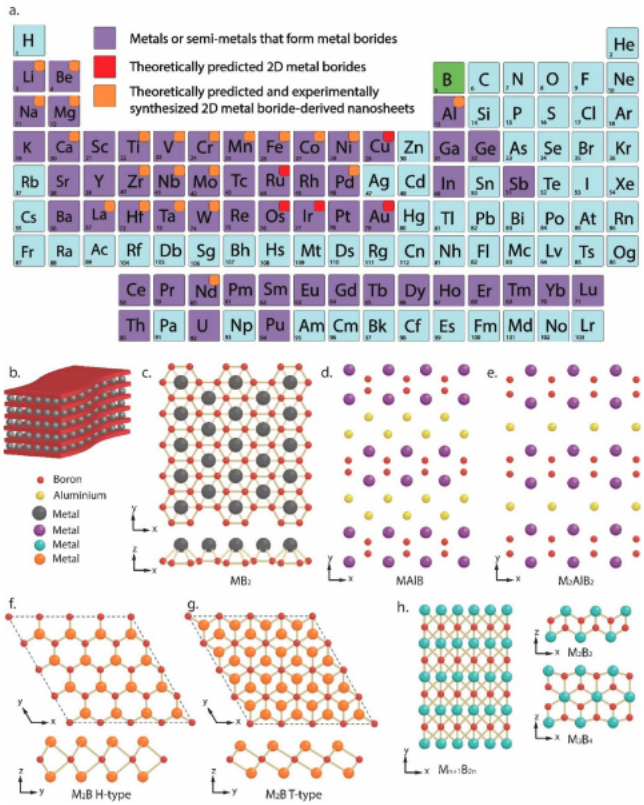

Figure 4: Metals forming borides and the structural patterns they exhibit. Periodic table displaying metals or semi-metals that produce borides of MBene and MAB phases, both theoretically and experimentally predicted [5]

.

First MBenes for LIBs have been discovered through theoretical calculations are Fe_2B_2, and Mo_2B_2 [63]. They feature an electronically conductive skeleton, strong chemical activity, and rapid charge carrier movement, making them more promising for energy storage applications. The chemical formula for the MAB phase, $M_{n+1}AB_n$, is as follows: "B" stands for boron, and n = 1 to 4. "A" represents elements III–V of the A-group (Si, Ge, Sn, As, Bi, Ga, In, Tl, and others). Where "M" is transition metals denoted by Ti, V, Nb, Ta, Cr, Mo, and others Al mono-layer and bi-layers can be used to divide M-B layers [64].

The layered structures of twenty of the MAB materials have been synthesized experimentally [32] such as FeB_2 [65] and MoB_2 [66]. Most of them have been theoretically studied their properties and application (as shown in Figure .4a) [67, 68]. In 2015, Ade and Hillebrecht [69] studied "7," the treble borides. The crystal structures of different MAB phases of (MAlB, M_2AlB_2, $M3Al_2B_2$, $M3AlB_4$, and M_4AlB_6) is portrayed in Figure .5 [70].

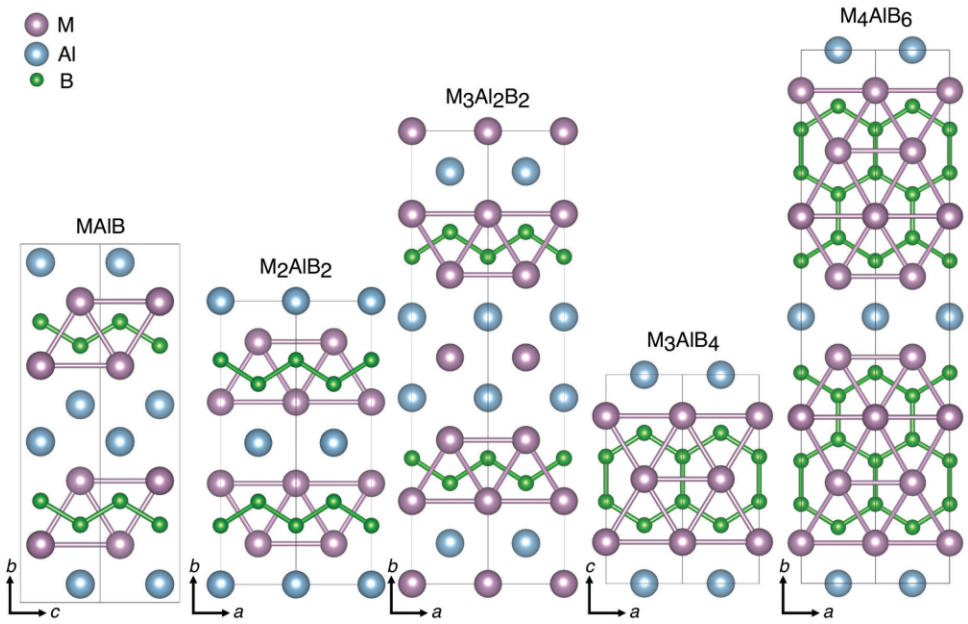

Figure 5: The different MAB phases of Crystal structures[6].

Using the crystal structure prediction approach reported on a series of hexagonal 2D MBenes, Zr_2B_2,Ti_2B_2, Mo_2B_2, Y_2B_2, and Sc_2 that were predicted to have good stability and excellent electronics conductivity. Others, such as Fe_2B_2, V_3B_2, Mn_2B_2, Cr_2B_2, and Mo_2B_2, were also expected to perform well as electrode materials in LIBs/NaIBs [71].

In addition to the orthorhombic configurations for the hexagonal crystal system TMB_2 has a family of stacked TMBs. These layered TMBs, which include graphene-like honeycomb boron layers, can be converted into 2D "sandwich" structures, such as OsB_2, FeB_2, MoB_2, and RuB_2, that are made up of two boron honeycomb sheets and an intermediate hexagonal plane of the TM atom (B-TM-B). Illustrates the numerous scientific contributions made in MBenes, which have validated their various uses and are being predicted both theoretically and empirically as show as in Figure .6 [7].

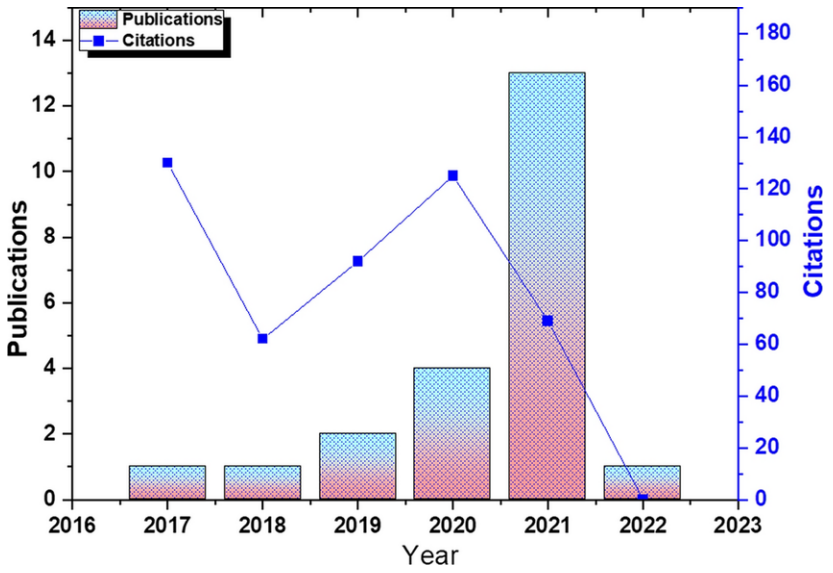

Figure 6: An overview of MBenes' research efforts. The volume of publications from 2017 to 2023 demonstrates a persistent rise in the subjects of interest for research [7].

2.4.1 The Mechanical and Dynamic Properties of MBene's

MBene 2D materials have higher elastic constants, Poisson's ratio, shear modulus of elasticity, and Young's modulus compared to other 2D materials. Calculations reveal that they increase mechanical properties [72]. The shear modulus measurements reveal the system's stiffness (softness) under cutting and responsiveness to shear stress. Young's modulus and Poisson's ratio were used to characterize the mechanical characteristics of MBenes monolayers. Furthermore, phonon spectroscopy is used to confirm the stability of crystal formations with lattice dynamics. If the Brillouin zone exhibits no imaginary frequency, 2D MBenes are dynamically stable. The computed MBene exhibited thermodynamic stability. Some of the monolayers include V_2B_2, Cr_2B_2, and Mn_2B_2, whose free energy oscillated slightly during the AIMD simulations at 350K [49].

2.4.2 The electronic Properties of MBene's

The electrochemical performance of MBenes electrodes for energy-related applications is influenced by their electronic properties. The electronic characteristics of MBenes have been investigated through both theoretical research and experimental characterisation. In a theoretical investigation, hybrid functionals were utilized to precisely determine the electronic band structure of MBenes, whereas the main electronic properties were computed utilizing the generalized gradient approximation (GGA) framework. Due to tightly coupled "d" orbital electrons in transition metal elements, Hubbard corrections between "2" and "6" eV were applied in related works.

Upon functionalization, most MBenes with non-terminated electronic structures exhibit metallic characteristics, with the Fermi energy situated in the transition metal's d band. The p-band of B appears below the d-band in the majority of MBenes, with a little bandgap between them. In $M_{n+1}B_n(n = 1, 2, 3)$ MBenes, the d-electrons of the transition metal atoms on the surface are crucial for the states close to the Fermi level. The electronic structures of the hexagonal monolayer of pristine and functionalized MBenes (M = Sc, Ti, Zr,

Hf, V, Nb, Ta, Mo, and W) with F, O, or OH groups have been thoroughly studied by Khaledialidusti et al. [73].

Without much experimental support, theoretical simulations have lately provided a description of MBenes, their electronic structure, and their optical characteristics. Non-functionalized Sc_2B_2, Ti_2B_2, V_2B_2, Cr_2B_2, Y_2B_2, Zr_2B_2, and Mo_2B_2 MBenes are identified as metallic by DFT calculations because the transition metal's 3d-orbitals occupy electronic states at the Fermi level [74].

The predicted band structure shows that, in contrast to the band connected to boron, the metal band has fewer transitions below the Fermi level. As a result, it is typically anticipated that in 2D MBenes, the degree of hybridization between atomic orbitals in the B-B bond will be comparatively higher than that of the M-B and M-M bonds. It is evident that F, OH, or O have higher electronegativity than the transition metals under study when comparing the predicted band structure of MBF, MBOH, and MBO with the pristine MB, and these termination groups have an impact on the electronic structure [7].

As first-principle calculations [75] show for Cr_2BO_2, $Cr_2B(OH)_2$, and $CrBCl_2$, a flat band appears near the Fermi level. Remarkably, ScBO has been expected to have semiconducting characteristics with an indirect bandgap of 0.5 eV, significantly correlated with the type of surface termination [76]. When MBenes terminate with $-$OH and $-$F groups, they lose their metallic or semimetal qualities; nevertheless, when they terminate with $-$O groups, they unexpectedly acquire semiconducting properties. The fundamental cause is because $-$O groups pull out more electrons from boron's π^* band states or from its occupied d states below the Fermi energy [76]. Consequently, MBenes seem promising for tuning band structures; this is especially true after surface functionalization.

2.4.3 Potential Effects of MBenes on Energy Storage

2D materials are used as anode materials in rechargeable batteries due to their outstanding mechanical qualities, high specific surface area, and excellent electron mobility. Many 2D

materials, including MoS_2 [21], graphene [77], and Ti_3C_2 [30], have been successfully explored as anode materials in recent years. The importance of theoretical computations in elucidating MBene's battery mode of action is becoming more and more important.

Recently, a theoretical study has projected a significant number of MBenes as potential anode materials for rechargeable batteries. Researchers often compute the structure, electrical characteristics, thermodynamic and mechanical stability, adsorption and diffusion properties of metal atoms on the MBene surface, open circuit voltage, specific capacity, and specific power energy in order to assess the performance of MBene as a metal ion battery electrode material.

2.4.4 Hetro-structure of MBene

A hetero-structure is a particular kind of hetero-structure that is made up of layers of one material and other materials layered on top of one another. These materials are utilized in the investigation of spin-valley coupling and valley polarization because they break inversion symmetry [78]. Hetero-structures are widely employed in conventional semiconductors to enhance their structural stability and tune the electrical and optical properties of one or 2D counterparts.

Van der Waals interactions in Hetero-structures have been identified as viable possibilities for the development of future 2D materials; prototype van der Waals Hetero-structures are TMD-based hybrid multilayered structures. According to recent reports, multilayered hetero-structures [79] MoS_2/MoB_2 [33], MoS_2/TiBF, and MoS_2/MoBO [80]. It must add below 5% of lattice mismatches in the smaller lattice constant of one of them due to different equilibrium lattice constants.

2.4.5 Application of MBene with theoretical and Experimental Synthesis

Rechargeable batteries' uses for energy storage and conversion (Figure 7). MBenes, a novel class of 2D , offer a wide range of potential uses as electrocatalyst for NRR and HER. It is also a compelling method of altering MBenes' structure to increase activity. MBenes composites

embedded in a single metal exhibit intriguing characteristics because of the monatomic and MBenes' respective high activity and electrochemical characteristics. In addition to electrocatalytic HER and NRR, MBene catalysts are novel nitric oxide and carbon dioxide reduction catalysts.

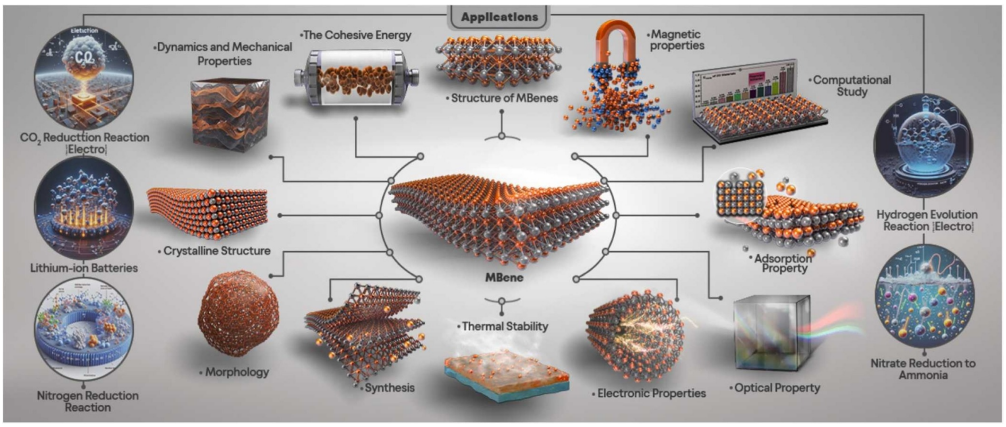

Figure 7: Main applications of MBenes with theoretical calculation [8].

Possible impacts of In the future, additional research in this area is required. Additionally, we concentrate on 2D MBene research for energy storage applications. MBenes have been noted to exhibit significant promise as anode materials for the upcoming battery generation. Researchers have also discovered that they have the greatest promise for biotechnology and the electrochemistry of technological industry. MBene materials have substantial contributions to energy storage and other uses via computational calculations.

The two-dimensional family of metal-organic frameworks, or MBenes, has grown in popularity because of its exceptional mechanical and electrical characteristics and distinctive structural kinds. It's also proven to have a wide range of applications in the field of energy storage and conversion. 2D MBenes are expected to be the brightest material in the future.

CHAPTER 3

RESEARCH METHODOLOGY

3.1 Schrödinger Equation

The Schrödinger equation is the goal of all computations using quantum mechanics and electronic structure techniques [81]. Because it makes the system's wave function visible, the Schrödinger equation is therefore essential to these methods as it allows the computation of all the system's physical characteristics. All information about the locations and spins of the particles that comprise the system is contained in the wave function[82]. We are given the time-independent Schrödinger equation by[83]:

$$\hat{H}\psi = E_{Total}\psi \tag{3.1}$$

where the system's Hamiltonian, or total energy, is represented by the operator $\hat{H}$. E stands for both the energy and the wave function that characterize the quantum state of the system. The observable material attribute of the materials that interest us can be found by solving this equation. After calculating the contributions of pure electron-electron, electron-nuclear, and nuclear-nuclear interactions to the total energy of the system, the following description of the system can be formed using the aforementioned equations [84]:

$$\hat{H} = T + T_n + V_{int} + V_{nn} + V_{ext} \tag{3.2}$$

Where:

- T= kinetic energy of the electrons,
- Tn= kinetic energy of the nuclei,
- Vint= potential energy of the inter-electron (electron-electron) repulsions,
- Vnn = potential energy of the nuclear-nuclear repulsions and
- Vext = potential energy of the electron-nuclear attraction (external potential)

$$\hat{H} = \frac{-\hbar^2}{2m_e}\sum_i \nabla_i^2 - \sum_I \frac{\hbar^2}{2M_I}\nabla_I^2 + \frac{1}{2}\sum_{i\neq j}\frac{e^2}{|\mathbf{r}_i - \mathbf{r}_j|} + \frac{1}{2}\sum_{I\neq J}\frac{Z_I Z_J e^2}{|\mathbf{R}_I - \mathbf{R}_J|} - \sum_{i,I}\frac{Z_I e^2}{|\mathbf{r}_i - \mathbf{R}_I|} \quad (3.3)$$

Now, the Schrödinger equation for several body systems can be solved with ease, notwithstanding its previous complexity. The spins and positions of the electrons in the system are now the only factors influencing the many-body wave function (ψ); the nuclear positions are only a part of the external potential (V_{text}).

3.2 Wave function-based approximations

3.2.1 The Born-Oppenheimer Approximation

In general, the Hamiltonian operator $\hat{H}$ depends on nuclear and electronic degrees of freedom. Because of the significant mass difference between electrons and nuclei, the Born-Oppenheimer approximation permits the separation of electronic and nuclear dynamics[85]. At almost 2000 times the mass of an electron, a nucleus is far heavier than an electron. As a result, electronic motion is three to five orders of magnitude quicker than nuclei motion; as a result, an electron's motion will be far faster than a nucleus'.Barrera et al. (2024): Emergent Because the nuclei are assumed to be fixed with certain coordinates ($\{R_I\}$), that is, they enter as external parameters, the many-body system's Hamiltonian can therefore be reduced to an N-electron Hamiltonian[86]. Therefore, adopting the Born-Oppenheimer approximation; equations (3.4) can be rewritten in terms of the electronic Hamiltonian $\hat{H}$ as[87]:

$$\hat{H}_{ele} = -\frac{\hbar^2}{2m_e}\sum_{i=1}^{N}\nabla_i^2 + \frac{1}{2}\sum_{i}\sum_{j\neq i}\frac{e^2}{|\mathbf{r}_i - \mathbf{r}_j|} + \sum_{I=1}^{M}\sum_{i=1}^{N}\frac{Z_I e^2}{|\mathbf{r}_i - \mathbf{R}_I|} + V_{ne} \tag{3.4}$$

or

$$H_{\text{ele}} = \hat{T}_{\text{e}} + \hat{V}_{\text{Ne}} + \hat{V}_{\text{ee}} \tag{3.5}$$

The complexity of solving the Schrödinger equation for many body systems is reduced to a tractable problem for the fact that $\Psi(R, r) \rightarrow \psi(r)$ thanks to the Born-Oppenheimer approximation and the ensuing simplification of the full Hamiltonian ($\hat{H}$) to the electronic Hamiltonian ($\hat{H}$). For many-electron systems, the Born-Oppenheimer approximation simplifies the issue, although it is still essentially unsolvable. Wave function-based techniques are practical and produce good results for small enough molecules. The whole electronic wave function cannot be determined from the product of wave functions for each electron inside three three-dimensional degrees of freedom due to the interaction of individual electrons in many-electron systems. This could also turn the difficulties of $\hat{H}$ into one of three dimensions in three dimensions. Numerous methods have been provided to solve equation (3.3).

The Hamiltonian is divided into two components by the Born-Oppenheimer approximation: the nuclear Hamiltonian $\hat{H}$nuc and the electronic Hamiltonian $\hat{H}$ele. Whereas the nuclear Hamiltonian is only dependent on the nuclear coordinates and the fixed electronic locations, the electronic Hamiltonian is only dependent on the electronic coordinates and the fixed nuclear positions. It is possible to further break down the electronic Hamiltonian into terms of potential and kinetic energy [88].

where:

$\hat{T}_{\text{e}}$ is the kinetic energy operator of the electrons, $\hat{V}_{\text{Ne}}$ is the potential energy operator of the electron-nucleus interaction, $\hat{V}_{\text{ee}}$ is the potential energy operator of the electron-electron repulsion, and $\hat{V}_{\text{nn}}$ is the potential energy operator of the nucleus-nucleus repulsion. The nuclear Hamiltonian can be expressed as:

$$\hat{H}_{\text{nuc}} = \hat{T}_{\text{N}} + \hat{V}_{\text{NN}} \tag{3.6}$$

where:

$\hat{T}_{\text{N}}$ is the kinetic energy operator of the nuclei, and $\hat{V}_{\text{NN}}$ is the potential energy operator of the nuclear-nuclear repulsion. In most cases, the nuclear Hamiltonian can be neglected as it primarily influences the vibrational and rotational motion of the molecule, which are considerably smaller in scale compared to the electronic motion[89].

3.3 Density Functional Theory

Density functional theory is a computational quantum mechanical modeling technique used to study the nuclear and electronic structure of many-body systems in the fields of physics, chemistry, and materials science. Atoms, molecules, and condensed phases are its main subjects. In addition to that, it makes it possible to solve the Schrödinger equation approximatively and precisely. Reformulating the electronic structure problem in terms of electronic density is the main concept rather than the many-body wave function $\Psi(\mathbf{r}_1\sigma_1, \mathbf{r}_2\sigma_2, ..., \mathbf{r}_N\sigma_N)$. The primary idea behind density functional theory is the great balance between computing expense and the accuracy with which electrons in a material can be described. It has grown in popularity and versatility in the fields of computational physics, condensed matter physics, and computational chemistry, based on the spatially dependent electron density.

In 1998, Walter Kohn and John Pople, two scientists, were recognized with the Chemistry Nobel Prize for their contributions to density functional theory and computational methods[90]. The most effective and accurate computing materials by using DFT because of improvements in approximations. Using the variational technique depends on the electronic density that controls the system's energy in the ground state. It can be used to study molecules, solids, atoms, nuclei, and both classical and quantum fluids [91]. The first significant developments

in the development of contemporary DFT were the Hohenberg-Kohn theorems and the work of Kohn and Sham.

3.3.1 Hohenberg and Kohn

In 1964, two incredibly simple theorems were stated and proved by Hohenberg and Kohn [92]. Hohenberg and Kohn introduced the idea of electron density $\rho o(r)$ [93] as a substitute for computing every interaction between electrons within the context of density functional theory (DFT). There are two theorems[94].

Theorem 1 *States that the ground state properties of a many-electron system are determined by its 3D electron density, $n(\mathbf{r})$. It also explains how all of the system's physical properties can be readily understood from a given Hamiltonian by solving the time-independent Schrödinger equation as functionals of the electronic charge-density, $n(\mathbf{r})$.*

Theorem 2 *It holds that $E_0 \leq E[\rho(\mathbf{r})]$ for any trial density $\rho(\mathbf{r})$ where the system's ground-state energy is denoted by E_0. Stated differently, the ground state energy of the system is represented by the smallest value of the total-energy functional $E[\rho(\mathbf{r})]$, and the single particle ground state density is precisely the density that provides this minimum value.*

The Hohenberg-Kohn theorems [95, 96] define the energy functional as

$$E[\rho(\mathbf{r})] = \int V_{\text{ext}}(\mathbf{r})\rho(\mathbf{r})d\mathbf{r} + F[\rho(\mathbf{r})] \tag{3.7}$$

The first term in equation (3.7), viewed from the right side, describes how the electrons interact with the external potential (V_{text}). The V_{text} phrase also includes the interactions of the nuclei with the system's electrons. The universal functional, $F[\rho(\mathbf{r})]$, is unknown as one cannot have all the information required to determine the ground-state energy of a many-electron system [97].

3.3.2 Kohn and Sham

In 1965, Kohn and Sham that The many-body quantum mechanical problem could be reduced to a system of one-electron equations with self-consistent solutions and precise equivalents. Overlaying the system of interacting electrons is an additional system of non-interacting electrons with the same ground state charge density, n(r). Through their reformulation of the basic equations to incorporate the most complex electron interactions into an "exchange-correlation functional," Kohn and Sham made practical applications possible. Although the exact form of this exchange-correlation function is not apparent, numerous types of materials have responded favorably to extensions and approximations based on electron gas models[95].

Kohn and Sham [98] implemented a method for solving equation (3.7) above for the unknown term, $F[\rho(\mathbf{r})]$. They did this by constructing a corresponding non-interacting system in some effective potential V_{eff} such that the non-interacting Hamiltonian produces the same ground state density $\rho_0(\mathbf{r})$' for any interacting ground state density $\rho_0(\mathbf{r})$. Equation 3.7 shows that, on the basis of this supposition, Kohn and Sham were able to dissect the unknown energy functional factor from the Hohenberg-Kohn theorem into many component terms.

$$F[\rho(\mathbf{r})] = E_{\text{ke}}[\rho(\mathbf{r})] + E_{\text{H}}[\rho(\mathbf{r})] + E_{\text{xc}}[\rho(\mathbf{r})] \tag{3.8}$$

Inserting equation 3.8 into equation 3.9, Kohn-Sham energy functional in DFT can be written as:

$$F[\rho(\mathbf{r})] = \int V_{\text{ext}}(\mathbf{r})\rho(\mathbf{r})d\mathbf{r} + E_{\text{ke}}[\rho(\mathbf{r})] + E_{\text{H}}[\rho(\mathbf{r})] + E_{\text{xc}}[\rho(\mathbf{r})] \tag{3.9}$$

wherein $[\rho(\mathbf{r})]$ $E_{\text{ke}}]$ the energy of a group of non-interacting electrons is described by the term, which denotes the electrons' kinetic energy, and $E_{\text{H}}[\rho(\mathbf{r})]$ the columbic energy of the electron-electron interaction is denoted by the word, which stands for the Hartree. The final element, $E_{\text{xc}}[\rho(\mathbf{r})]$, represents the energy contribution from exchange and correlation of electrons inside the interacting systems.

The Hartree energy which could be defined as

$$E_{\mathrm{H}}[\rho(\mathbf{r})] = \frac{1}{2}\iint \frac{\rho(\mathbf{r})\rho(\mathbf{r}')}{|\mathbf{r}-\mathbf{r}'|} d\mathbf{r} d\mathbf{r}' \tag{3.10}$$

has no contribution in the case of electron-electron correlational interacting energy. On the other hand, the assignment of minimizing such unknown exchange correlational functional would be simplified in the form of the Euler-Lagrange equation [96]:

$$\left\{ E[\rho(\mathbf{r})] - \mu \int \rho(\mathbf{r}) d\mathbf{r} \right\} = 0 \tag{3.11}$$

$$\frac{\delta E[\rho(\mathbf{r})]}{\delta \rho(\mathbf{r})} = \frac{\delta}{\delta \rho(\mathbf{r})} \left\{ \int V_{\mathrm{ext}}(\mathbf{r})\rho(\mathbf{r}) d\mathbf{r} + E_{\mathrm{ke}}[\rho(\mathbf{r})] + \frac{1}{2}\iint \frac{\rho(\mathbf{r})\rho(\mathbf{r}')}{|\mathbf{r}-\mathbf{r}'|} d\mathbf{r} d\mathbf{r}' + E_{\mathrm{xc}}[\rho(\mathbf{r})] \right\} \tag{3.12}$$

$$\mu = \frac{\delta E[\rho(\mathbf{r})]}{\delta \rho(\mathbf{r})} = \frac{\delta E_{\mathrm{ke}}[\rho(\mathbf{r})]}{\delta \rho(\mathbf{r})} + V_{\mathrm{ext}}(\mathbf{r}) + \int \frac{\rho(\mathbf{r}')}{|\mathbf{r}-\mathbf{r}'|} d\mathbf{r}' + \frac{\delta E_{\mathrm{xc}}[\rho(\mathbf{r})]}{\delta \rho(\mathbf{r})} \tag{3.13}$$

$$\mu = \frac{\delta E[\rho(\mathbf{r})]}{\delta \rho(\mathbf{r})} = \frac{\delta E_{\mathrm{ke}}[\rho(\mathbf{r})]}{\delta \rho(\mathbf{r})} + V_{\mathrm{ext}}(\mathbf{r}) \tag{3.14}$$

Here we combined together all terms, excepting non-interacting electron kinetic energy, into an effective potential $\hat{V}_{eff}(\mathbf{r})$ depending upon $\mathbf{r}$ [96]:

$$\hat{V}_{eff}(\mathbf{r}) = \hat{V}_{ext}(\mathbf{r}) + \frac{1}{2}\int \frac{\rho(\mathbf{r}')}{|\mathbf{r}-\mathbf{r}'|} d\mathbf{r}' + \hat{V}_{xc}(\mathbf{r}) \tag{3.15}$$

here, the last term of equation (3.15), $\hat{V}_{xc}(\mathbf{r})$, is the exchange-correlation potential and related to exchange-correlation energy functional, $E_{xc}[\rho(\mathbf{r})]$, by [96]

$$\hat{V}_{xc}(\mathbf{r}) = \left(\frac{\delta E_{xc}[\rho(\mathbf{r})]}{\delta \rho(\mathbf{r})} \right) \tag{3.16}$$

On account of equation (3.16), one would give a solution to the Schrödinger equation for

non interacting particles of the form [96],

$$\left[-\frac{\hbar^2}{2m_e}\nabla^2 + V_{eff}(\mathbf{r})\right]\phi_i(\mathbf{r}) = E_i\phi_i(\mathbf{r}) \tag{3.17}$$

where the parameters E_i, $\phi_i(\mathbf{r})$ and $\hat{V}_{eff}$ respectively indicate the orbital energies. The system's effective potential and non-interacting electrons are located in the Kohn and Sham orbitals. Everyone would agree that DFT offers a way to solve the Schrödinger equation for a particular system, which may be made feasible by combining the Kohn-Sham equation with the Hohenberg-Kohn theorems. The first step in the iterative process of solving a problem is to estimate the electron density ($\rho(\mathbf{r})$), which is then used in equation (3.15) to create an effective potential ($\hat{V}_{eff}$) term. This effective potential term can be entered into equation (3.16), which will produce a set of Kohn-Sham orbitals for the system. This makes it possible to get an improved estimate of the electron density, $\rho(\mathbf{r})$, using equation (3.17). [96].

$$\rho(\mathbf{r}) = \sum_i |\phi_i(\mathbf{r})|^2 \tag{3.18}$$

The previous analytical discussion can also be condensed using the flow graphic that follows.

As seen in Figure.8 below, this iterative cycle would be continued until convergence upon a single value for the electron density, at which point one would obtain an improved estimate of the electron density ($\rho(\mathbf{r})$). The ground-state electron density for the system and all of its physical properties could be determined using the second Hohenberg-Kohn theorem [95] if the electron density converged in accordance with the self-consistent field method previously described. The flow chart would continue if the electron density did not converge.

The self-consistent field method involves solving the Hartree-Fock equations to determine the optimal one-electron wavefunctions for a many-electron system. The Fock operator is built from the electron density and the external potential, while the electron density is derived from the Slater determinant of the one-electron orbitals. After then, the Fock operator is

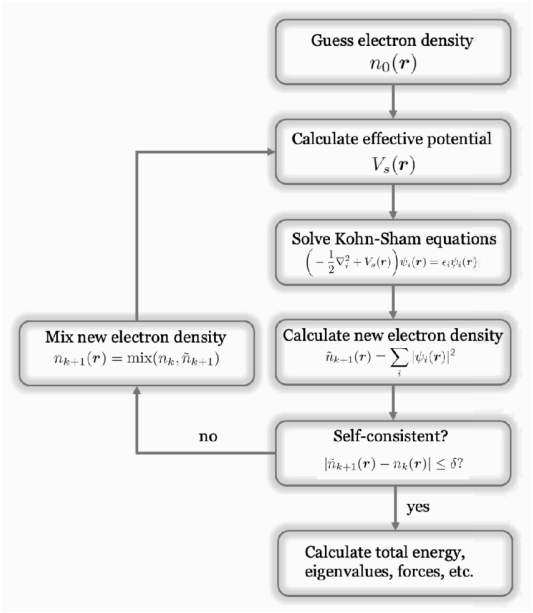

Figure 8: An simplified flowchart that shows how to solve KS equations using the self-consistency loop [9].

diagonalized to produce new orbitals and energies. This procedure is continued until the electron density approaches a stable value. Hartree-Fock theory and Kohn-Sham density functional theory are two applications of the self-consistent field approach.

The Hohenberg-Kohn theorems are two key findings in density functional theory that prove the variational principle for energy functional minimization as well as the existence and uniqueness of a universal energy functional of the electron density. According to the second Hohenberg-Kohn theorem, the ground-state electron density that minimizes the energy functional is the same as the system's exact ground-state energy. The theoretical underpinning for use electron density as the fundamental variable in computations involving quantum chemistry is provided by the Hohenberg-Kohn theorems.

3.4 Exchange Correlation Functionals

The approximation of the exchange-correlation energy functional $E_{xc}[\rho(r)]$ part of equation (3.15) mentioned above is seen as a major source of error for current DFT computations.

Therefore, obtaining a reliable approximation of this amount is crucial to the correctness of the entire DFT technique. Many different strategies have been used to solve this issue, but opinions are still divided on whether the best estimate for this term is obtained solely theoretically or semi-empirically. This issue may be seen using a Jacob's ladder, as seen in Figure 9 [10]. The visual ladder that raises the accuracy of DFT approximations from the so-called "Earth of Hartree," where exchange and correlation energies are completely ignored as in the Hartree approximation, to the chemical accuracy "heaven" corresponds to different classes of functionals and methods. More sophisticated higher step approaches will often require more processing power in this basic ranking of methods in exchange for improved calculation accuracy.

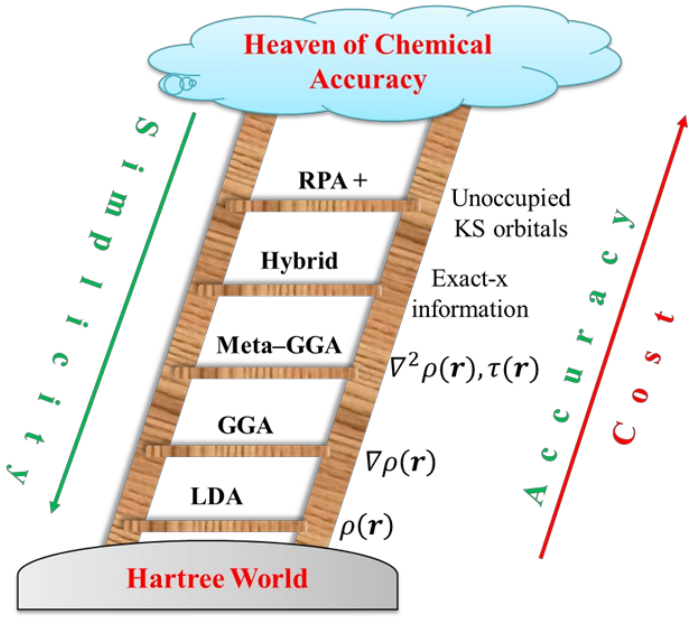

Figure 9: Different classes of DFT approximations are ordered by increasing levels of sophistication going up the ladder. Rungs are named at the center and the added components are noted on the right. ρ is electron density [10].

Local Density Approximation (LDA) The first and most used approximation for the exchange-correlation interaction (LDA) is the local density approximation (LDA)[99]. The exchange-correlation of the system was taken to be equal to that of a uniformly dispersed electron gas with density $n(\mathbf{r})$. The local density approximation for a homogeneous electron

gas is expressed as follows [100]:

$$E_{LDA}^{XC}[n] = \int n(\mathbf{r})\epsilon_{\text{unif}}^{XC}(n(\mathbf{r}))d^3\mathbf{r} \tag{3.19}$$

Where: $\epsilon_{\text{unif}}^{XC}$ is known as the exchange-correlation energy per particle of a homogeneous electron with density n in the electron gas. While some aspects of lattice constant equilibrium geometries and vibrational frequencies are described using LDA, other properties like as cohesive energies and dissociation energies of molecules are not represented, the LDA has a decent approximation for slowly charging densities[101].

Generalized Gradient Approximation (GGA) The second method of exchange-correlation interaction is the Generalized Gradient Approximation (GGA), which takes into account the non-uniform nature of the electron density by replacing the exchange-correlation of a homogeneous electron density with the semi-local function of the electron density and the gradient's magnitude [102].

$$E_{GGA}^{XC}[n] = \int d^3r f(n(\mathbf{r}), \nabla n(\mathbf{r})) \tag{3.20}$$

where, additionally, f is an analytical function that has multiple parameterization options. For general uses, Perdew-Burke-Ernzerhof (PBE) is one of the most often utilized functionals. GGA is a more accurate method than LDA for predicting binding energies, lattice constants of different materials, and activation energies of chemical processes. Based on the generalized gradient approximation (GGA) that Perdew-Burke-Emzehof provided for our computation (PBE), let us examine the exchange-correlation functional.

3.5 Density Functional Dispersion Correction

The dispersion correction energy factor is a very straightforward function of interatomic distances with adjustable parameters that is fitted to the structural and interaction energies

calculated using a complete basis set (CBS). Fitting is finished for a particular purpose. All atom pairs are considered in the energy corrections for DFT-D2 [103]. Furthermore, as an add-on factor, the dispersion correction has no direct impact on the wavefunction or any other molecular features. However, geometry optimizations with dispersion correction will provide a different geometry than those without it because of its contribution to the forces operating on the atoms[104].

The long-range attractive interactions between molecules that are poorly characterized by traditional density functional theory (DFT) can be taken into account with the help of dispersion correction. Dispersion correction can be applied in a variety of ways, including by incorporating dispersion effects into the exchange-correlation function, adding an empirical pairwise potential to the DFT energy, or employing a hybrid strategy that combines the two.

The dispersion energy and the self-consistent Kohn-Sham-DFT (KS-DFT) energy, E_{DFT}, are added to determine the total energy E_{D2} [105, 106] and E_{D3} [107, 108], respectively. DFT energy as follows [109]:

$$E_{DFT-D2} = E_{KS-DFT} + E_{disp} \tag{3.21}$$

where

$$E_{\text{disp}} = -s_6 \sum_{i=1}^{N_{\text{at}}-1} \sum_{j=i+1}^{N_{\text{at}}} C_{ij} \frac{1}{R_{ij}^6} f_{\text{dmp}}(R_{ij}) \tag{3.22}$$

and $f_{\text{dmp}}$is the damping function given by:

$$f_{\text{dmp}}(R_{ij}) = \frac{1}{1 + e^{-d(R_{ij}/R_r - 1)}} \tag{3.23}$$

The number of atoms in the system is denoted by N_{at}, the interatomic distance is denoted

by R_{ij}, the dispersion coefficient for the pair of atoms i and j is calculated using geometric mean of the form $C_{ij}^6 = \sqrt{C_i^6 \cdot C_j^6}$, and the global scaling factor is commonly denoted by s_6. For PBE, $s_6 = 0.75$, R_r is the sum of the atomic van der Waals radii, d is the damping parameter, and f_{damp} is a damping function that, in order to prevent overestimation, lowers the dispersion contribution at short distances. For a set of molecules, the dispersion coefficients and the damping function parameters are determined by fitting high-level theoretical or experimental data [110].

DFT-D2 is an easy-to-use and efficient method of increasing the accuracy of DFT for systems with dispersion-dominated interactions, molecular crystals, biomolecules, and van der Waals complexes. Nevertheless, DFT-D2 has certain drawbacks, including the omission of many-body effects, higher-order factors in the dispersion energy expansion, and the dependency of the dispersion coefficients on the local environment. More sophisticated dispersion correction techniques, like many-body dispersion (MBD)[111, 112], DFT-D3, and DFT-D4 can solve these problems.

3.6 Beyond Density Functional Theory

As it is well known, the PBE and LDA approximations both underestimate semiconductor materials' band gaps and provide an erroneous picture of the band structure of strongly correlated materials. The DFT+U method, the hybrid functional (HSE06) approach, the self-interaction correlation (SIC) method, and the DFT+DMFT method are some of the techniques used to handle the correlation of electrons [113]. The results shown in this dissertation[114] are also not obtained using hybrid functionals since they are computationally very demanding.

Accurate results for strongly correlated localized states, such as the d- and f-type orbitals of transition metal electrons and rare-earth elements, were treated using the DFT+U approach. This technique uses the on-site Hubbard U correction to treat self-interaction. where it was

better to take into account the higher correlations between the localized electrons and the Hubbard U parameter, which increased the Coulomb repulsion between them[115]. The entire DFT+U functional energy expressed as follows[116, 117];

$$E_{DFT+U}[n(\mathbf{r})] = E_{DFT}[n(\mathbf{r})] + E_U[n^m_{I,\sigma}] - E_{dc}[n_{I,\sigma}] \tag{3.24}$$

where: E_{DFT} is the DFT energy term, $n(\mathbf{r})$-electron density; $n^m_{I,\sigma}$ the atomic orbital occupations with spin σ for correlated atom I; E_U is the on-site Hubbard U correlation energy and E_{dc} express the double counting term.

The DFT+U technique involves augmenting the exchange-correlation functional with an on-site Coulomb repulsion term U in order to rectify the self-interaction mistake in DFT. U's value is determined by selecting the localized orbitals that characterize the Hubbard manifold. This can be done from the ground up using a variety of methods, including the self-consistent DFT+U method, the constrained random phase approximation, and the linear response method[118]. DFT+U opens the band gap, increases the magnetic moments, and stabilizes the proper ground state to better describe systems with strongly correlated electrons, such as actinides, lanthanides, and transition metal oxides. [119].

3.7 Nudged Elastic Band Method

For researching the kinetics and mechanisms of many different processes, including chemical reactions, ionic diffusion, surface diffusion, and phase transitions, the NEB technique is an effective tool. The Arrhenius equation can be used to determine the process's frequency using the activation energy that was determined by the NEB technique. Notwithstanding its potential benefits, the NEB technique presents certain drawbacks and difficulties. These include reliance on the starting and end states, spring constant selection, and the potential for many pathways and saddle points to exist[120, 121]. Therefore, it's crucial to use alternative techniques, like harmonic transition state theory or molecular dynamics simulations,

to confirm the accuracy and dependability of the NEB results.

The curve that connects two (meta)stable states of a system and has the lowest energy at each point along the curve is known as the **minimal energy path (MEP)** in physics and chemistry [122]. The MEP is helpful for researching phase transitions, transition mechanisms, and rates of other dynamical processes such as chemical reactions. The transition state, which represents the greatest energy barrier the system must cross to change from one state to another, is the highest point along the MEP [123].

The **nudged elastic band (NEB) method** is one of the most often used techniques to determine the MEP and the transition state. By using a sequence of discrete pictures, or beads, connected by springs and subjected to forces coming from the potential energy surface, the NEB technique approximates the MEP.

3.7.1 Principle of NEB method

The pictures' placements are iteratively optimized by the NEB approach until they converge to the MEP. An illustration of the NEB approach used on a basic two-dimensional potential can be found in Figure 10. Examine the potential energy surface that is shown. Two local minima are identified as the beginning and end states, and two lines—one a straight band and the other a curved MEP band—connect them. The arrows will direct us to begin our search in a straight line, and our goal is to reach the MEP line as soon as possible.

3.7.2 The Procedure of the NEB method

Initial and final states

The initial and final states of interest must first be determined using the standard electronic and ionic relaxations. These two configurations have low energies and all of the forces (first derivatives of the energy) are zero.

An atom that is within or on the surface of a lattice advances to the following location. As indicated in the following graphic, atoms must climb the potential mountain and descend

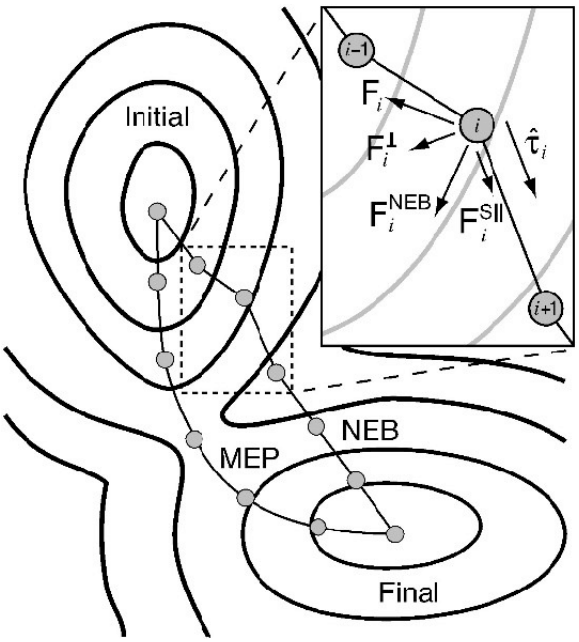

Figure 10: Principle of NEB method showing the initial band (dotted line) of three intermediate images, nudging toward the minimum energy path (MEP, solid line) which passes over the saddle point with barrier (activation) energy[11].

to the next position from their most stable location, which has the lowest potential energy. when The activation energy to move is Δ E. The mountain's height and the activation energy are equal. The Nudged Elastic Band (NEB) computation is the method used by DFT to determine activation energy.

3.8 Pseudopotentials

If electrons are separated into two groups—valence electrons and inner core electrons—the many-electron Schrödinger equation can be greatly simplified. The electrons in the inner shells create an almost inert core with the nucleus because they are tightly bonded and do not contribute much to the chemical bonding of atoms. They also partially screen the nucleus. Particularly in metals and semiconductors, valence electrons are virtually entirely responsible for binding characteristics. With the atom reduced to an ionic core that communicates with the valence electrons, this distinction means that the inner electrons can often be disregarded. Fermi and Hellmann were the first to suggest using an efficient interaction, or

pseudopotential, to simulate the potential experienced by the valence electrons in 1934 and 1935, respectively. Despite the mathematical simplification that pseudo-potentials provide, they were not widely used until the late 1950s [124, 125].

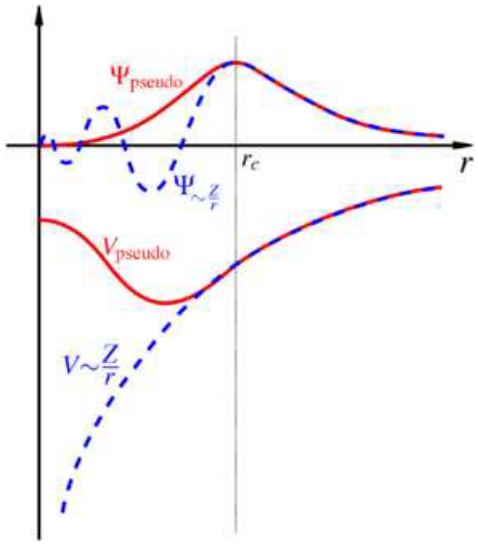

Figure 11: Schematically, the pseudopotential is represented by solid lines, while electrons are represented by dashed lines, both with the corresponding wave functions. The symbol rc stands for the cutoff radius that separates the core and valance zones [12]

3.9 The overall setup for the computation

The density functional theory (DFT) method was employed to calculate the interactions between different hetero-structure of Graphene/molybdenum diboride (MoB_2) and hetero-structure Graphene/ FeB_2 and various lithium Li_n ($n = 1, 2, and, 3$) clusters by using the Vienna Ab initio Simulation Package code (VASP) [13, 126]. The exchange-correlation potential was described by Perdew-Burk-Ernzerhof (PBE) generalized gradient approximation (GGA) functional. The wave function was expressed by plane wave basis with a cutoff energy of 500eV.

The convergence criterion of electron energy and ionic force were adopted with 10^{-5} eV and 0.05 eV/Å. Monkhorst-Pack k-point grid with $5 \times 5 \times 1$ (001) the surface of hetero-structure of both graphene/MoB_2 and Graphene/FeB_2 separately. The HS by reducing the lattice

mismatch between the two layers to 2.16% and 1.16% respectively. This lattice mismatch is small enough that will not effect the electronic characterises of the hetero-structure, however such contraction in lattice spacing's may results in increased DOS [127].

Table 1: Electron Configurations and Pseudopotential Types of Various Atoms

Atom	**Electron Configuration**	**Pseudopotential Type**
Fe	$3s^2 3p^6 4s^2 3d^6$	Ultrasoft
Mo	$4s^2 4p^6 5s^1 4d^5$	Ultrasoft
B	$2s^2 2s^2 2p^1$	Ultrasoft
C	$2s^2 2p^2$	Ultrasoft
Li	$1s^2 2s^1$	Ultrasoft

The lattice mismatch equation is expressed as follows:

$$\epsilon\% = \frac{a_{hetero-structure} - a_{pristine}}{a_{pristine}} \times 100 \tag{3.25}$$

Where $a_{hetero-structure}$ and $a_{pristine}$ are the lattice constants of the hetero-structure and pristine MBenes, respectively.

For the electronic structure, the calculation considered HSE06,[128, 128, 129]. The van der Waals correction of Grimme (D3) was used because of the weak interactions at the hetero-structure interface. To prevent interactions between the periodically repeated images along the Z axis, a 20$\mathring{A}$ vacuum gap was established.

Adsorption energy of lithium atoms on hetero-structures and pristine MBenes as follows:

$$\Delta E_{\text{ad}} = \frac{1}{n}[E_{\text{Li}_n\text{graphene/MBene}} - (E_{\text{graphene/MBene}} + E_{\text{Li}_n})] \tag{3.26}$$

where $E_{\text{Li}_n\text{graphene/MBene}}$ is the total energy of hetero-structure or pristine MBenes with intercalation, $E_{\text{graphene/MBene}}$ is total energy of graphene/FeB_2 or graphene/MoB_2 without intercalation or FeB_2 and MoB_2 pristine MBenes and E_{Li_n} is the total energy of the Li atom.

The formation energy of graphene/FeB2 and graphene/MoB_2 hetero-structures were calcu-

lated using the following equation:

$$\Delta E_{\text{bind}} = E_{\text{graphene/MBenes}} - E_{\text{graphene}} - E_{\text{MBenes}} \tag{3.27}$$

Where: $E_{\text{graphene/MBenes}}$, E_{graphene} and E_{MBenes} are the total energy of hetero-structure, pristine of graphene and MBenes (FeB_2 or MoB_2), respectively.

To determine the electrochemical properties of the Li adsorption process into the graphene/FeB_2 and graphene/MoB_2 hetero-structures, the Open-circuit voltage (OCV) were calculated using the following equation:

$$OCV = -\frac{1}{ne}\left[E_{\text{Li}_n\text{graphene/MBene}} - \left(E_{\text{graphene/MBene}} + nE_{\text{Li}}\right)\right] = -\frac{1}{ne}\Delta E_f \tag{3.28}$$

Where: $E_{\text{Li}_n\text{graphene/MBene}}$, $E_{\text{graphene/MBene}}$, E_{Li}, ΔE_f, n and e are the total energy of hetero-structures after intercalation of n atoms of Li per formula unit, the total energy of hetero-structure without intercalation species, the chemical potential of intercalated species of Li atom, formation energy, and the number of Li atom intercalation and elementary charges, respectively.

The theoretical capacity of LIBs is obtained from the following equation:

$$C_M = \frac{nx_{\max}F}{M_{\text{Hetero}}} \tag{3.29}$$

Where: n represents the amount of electrons transferred per formula unit (1 for Li), $x_{\max}$ represents the number of Li atoms adsorbed; in our calculation, $x_{\max} = 3$, F represents the Faraday constant ($26801 mAh/mol$), and M_{Hetero} represents the mole weight of graphene/FeB_2 and graphene/MoB_2 hetero structure or pristine MBenes.

The diffusion rate (r) and diffusion coefficient (D) of lithium ions are calculated using the following equations, where the activation energy (E_a) for each diffusion path is the difference

between the energy of the saddle point and the initial state:

$$r(T) = v \exp\left(-\frac{E_b}{k_B T}\right)$$
$$D = a^2 v \exp\left(-\frac{E_b}{k_B T}\right), \tag{3.30}$$

where k_B is the Boltzmann constant, T is the absolute temperature, and v is the hopping rate ($v = 10^{13}$ s^{-1}). At a temperature of 300 K, and assuming $k_B = 8.17333262 \times 10^{-5}$ eV/K, the diffusion coefficient for different E_b values can be calculated.

CHAPTER 4

RESULTS AND DISCUSSION

4.1 Structural properties

4.1.1 Lattice Constants and Bond Lengths of Monolayers systems

Lattice constants and bond lengths are computed by scientists studying materials like MoB_2, FeB_2, and graphene monolayer in order to comprehend its structural Characteristics. To validate the conclusions, these computations are frequently compared with experimental data and findings from other computational investigations. The dimensions of the unit cell, which are essential to the crystal structure of MoB_2, are shown by the lattice constants. The strength and kind of chemical bonds that are present can be inferred from the bond lengths between boron atoms and molybdenum (Mo), which in turn influences the qualities of the material.

Likewise, for FeB_2, the lattice constants provide insight into the general structure of the iron (Fe) and boron atoms. The potential hardness and electrical characteristics of the material can be inferred from the link lengths between atoms of boron and iron. Last but not least, the lattice constant is the distance between carbon atoms in a monolayer of graphene. The remarkable strength and conductivity of the material are largely dependent on the length of the link between carbon atoms.

Table 2: Calculated lattice constants and bond lengths of FeB_2, MoB_2, and graphene monolayers of an atom compared with the experimental result and computational study.

System	Lattice constant (Å)	Bond lengths in (Å)					Reference
		Mo-B	Fe-B	B-B	C-C	Mo-Mo	
MoB_2	a = b = 3.045, c = 3.071	2.42	-	1.75	-	3.03	expe[130, 131]
		2.31	-	1.68	-	2.91	[132, 133]
	a=b= 3.019, c=20.961	2.42	-	1.75	-	-	[134]
	a=b=3.03 , c= 20.000	2.304	-	1.750	-	3.03	This work
FeB_2	a = b = 3.015, c = 20.000	-	1.93	1.82	-	-	expe[135, 136]
	a = b = 3.020, c = 2.692	-	2.22	1.74	-	-	[132, 137]
	a = b = 3.015, c = 20.000	-	1.886	1.744	-	-	This work
Graphene	a = b = 2.46	-	-	-	1.42	-	Expe[138, 139]
	a = b = 3.015, c =2.739	-	-	-	1.8	-	[140, 141]
	a = b = 2.468, c =20.000	-	-	-	1.425	-	This work

4.1.2 Optimize Structure of Monolayers systems

The figure (12) shows a monolayer, which is made up of just one layer of molecules or atoms stacked on a surface. Here, we see an arrangement of atoms in two dimensions. Atoms of boron (B) are represented by the green spheres, and atoms of iron (Fe) are represented by the gold spheres. The other monolayer of graphene represented by brown. The monolayer structure is formed by the arrangement of these atoms. The word "optimized" denotes that certain properties have been attained or the energy of the system has been reduced by adjusting the atomic locations.

Atomic locations are changed during optimization to improve stability, electrical characteristics, or other desired features. Panel A and E (Side View) presents a cross-sectional view that reveals the bonding patterns and demonstrates how the atoms stack vertically. In summary, the figure illustrates an optimized monolayer structure composed of boron and iron atoms. This transition from a simple linear arrangement (Panel A and E) to a complex lattice (Panel B and F) likely involves adjustments to achieve desirable electronic or mechanical properties.

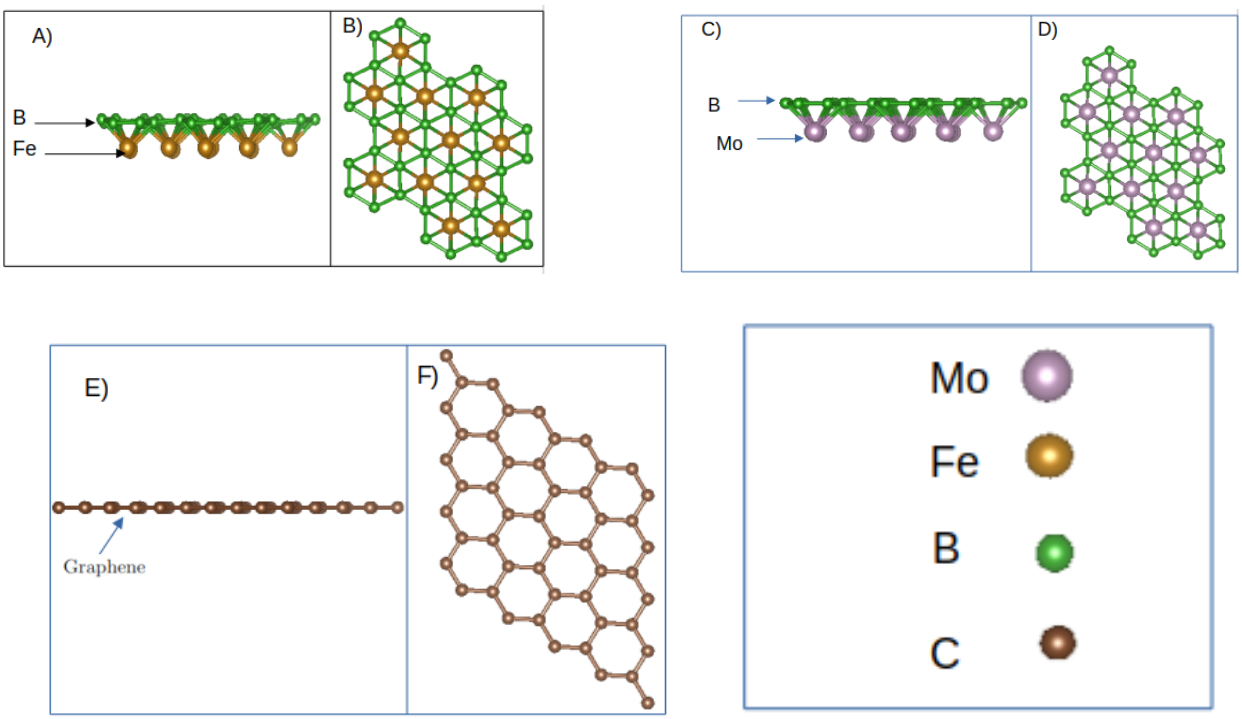

Figure 12: Te.

4.1.3 Optimize Hetero-structure of the materials

Figure 13 illustrates the hetero-structure that is significant for the study of lithium-ion batteries. The hetero-structure is composed of a monolayer of FeB_2, where boron (B) atoms are depicted as green spheres and iron (Fe) atoms as gold spheres, and an instade of FeB_2 replaced with MoB_2, where molybdenum (Mo) atoms are as purple spheres. This monolayer is intricately arranged above a layer of graphene, represented by brown. The side view (Panel A, C, E, and G) and top view (Panel B, D, F, and H) provide different perspectives of this optimized structure, and vice versa, graphene below with the layers of FeB_2 and MoB_2, respectively.

The optimization of such a monolayer is crucial for enhancing the performance of lithium-ion batteries. The FeB_2 and MoB_2 monolayers, with their unique arrangements of boron and iron atoms and also molybdenum, offer potential sites for lithium adsorption, which is a key factor in the battery's charge and discharge processes. The graphene layer contributes to the

overall stability and conductivity of the hetero-structure, making it an excellent candidate for electrode materials in lithium-ion batteries.

In-depth investigations employing density functional theory (DFT) are necessary to comprehend this hetero-structure's electrical characteristics and lithium adsorption behavior. The energy levels, charge distributions, and possible routes for lithium ions inside the structure can all be understood by DFT simulations. Predicting the behavior of novel materials and directing the creation of more robust and efficient lithium-ion batteries are made possible by these theoretical investigations. Thus, the figure the intricate relationship between theoretical physics and materials research, which has the potential to advance energy storage technology.

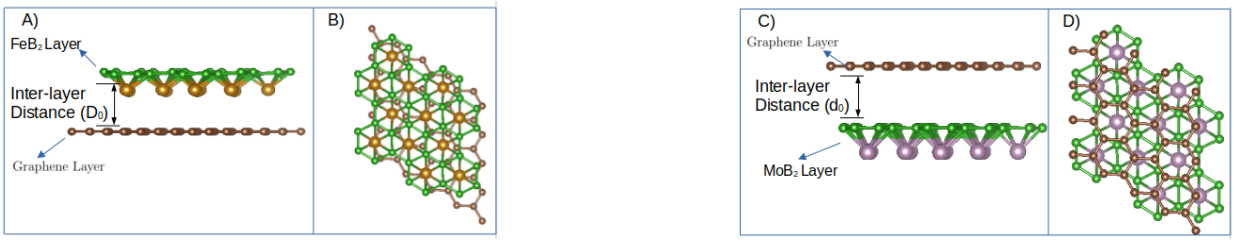

Figure 13: The optimized structures of MBene Based hetero-strucures. A) side view of B_2Fe/graphene. B)Top view of B_2Fe/graphene. C) side view of graphene/B_2Mo. D) Top view of graphene/B_2Mo.

Figure 14: The optimized structures of MBene Based hetero-strucures. (E) side view of graphene/B_2Fe. F) Top view of graphene/B_2Fe. G) side view of B_2Mo/graphene. H) Top view of B_2Mo/graphene

4.2 Electronic Properties of Monolayer Systems and Hetero-structure

The electronic properties of the electrode materials are described by the band strucure, density of states (DOS) and project density of states (PDOS) calculations. Metallic conductivity makes for the best electrode material for use in batteries, and it may be identified by crossed bands in Fermi-level existing states.

4.2.1 Total Desity states and Project Density of States (PDOS)

The projected density of states (PDOS) plots for FeB_2 and MoB_2 reveal the specific atomic orbitals contributing to their electronic properties. The d orbitals of iron (Fe) and the p orbitals of boron (B) atoms greatly influence the electronic bands in FeB_2. Similarly, in MoB_2, the valence and conduction bands are affected by the d orbitals of molybdenum (Mo) and the p orbitals of boron (B) atoms. The Fermi level intersects the total density of states (DOS) plot at 0 eV, indicating metallic behavior. PBE+D3 computation is the key to accurate predictions.

The PDOS for graphene mostly reflects the p orbitals of carbon atoms. The fact that graphene is metallic, with the Fermi level at 0 eV, is further supported by the total DOS plot. The HSE06 computation approach provides insights into detailed electronic structures. When constructing materials with desired electrical properties, these DOS and PDOS graphs are extremely important. It is critical to comprehend these electrical characteristics in applications such as lithium-ion batteries, where conductivity and stability are important. The Fermi level in the plots is referenced by the green broken line at 0 eV, and reliability is increased by using sophisticated techniques like PBE+D3 and HSE06.

The electronic structures of FeB_2[36], MoB_2[142, 143, 144], and graphene[] are promising for Li-ion battery applications. The presence of d orbitals in the conduction band of FeB_2 and MoB_2 suggests a high capacity for lithium intercalation. graphene[145, 146], with its superior conductivity, can significantly enhance the electrode's performance by providing a conductive network for electron transport which is consistent with the previous study.

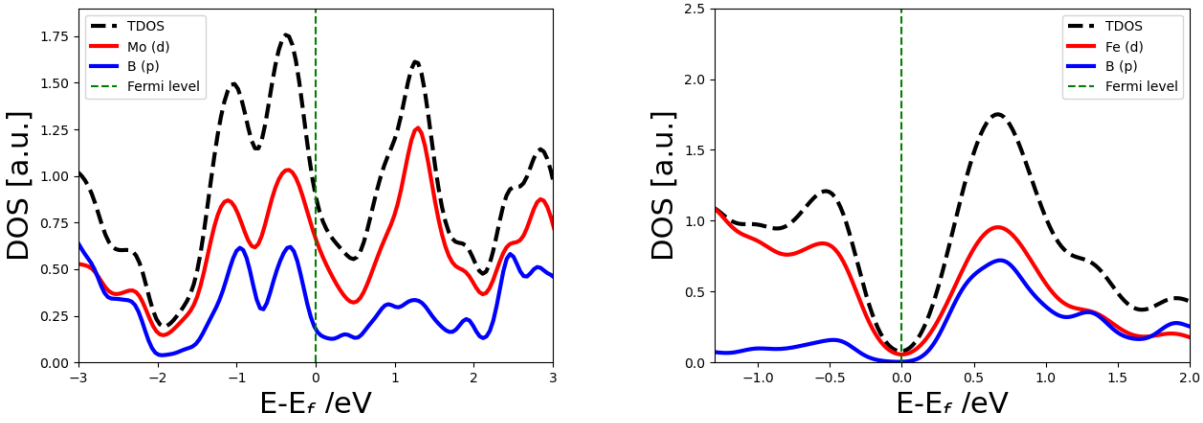

(a) FeB_2 (b) B_2Mo

Figure 15: The total density of states and project density state for(a) FeB_2 and (b)MoB_2 monolayers. The Fermi level is indicated by the green color broken line at 0 eV. The PBE+D3 calculation is employed.

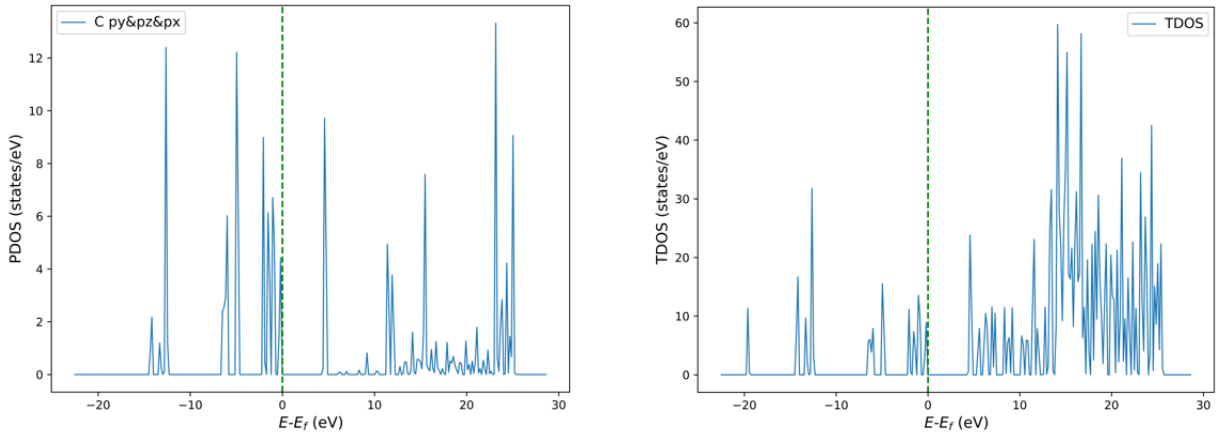

(a) Graphene (b) Graphene

Figure 16: (a)The project densities of states and (b)The Total densities of states for graphene monolayer. The Fermi level is indicated by the green color broken line at 0 eV. The HSE06 calculation is employed

So that, the studied monolayers, including graphene, exhibit metallic characteristics due to the Fermi level aligning with the zero electronvolt (eV) energy mark. These properties are advantageous for Li-ion battery electrodes, as they promise improvements in charge capacity, energy efficiency, and rate This study explores the electronic properties of graphene, FeB_2, and MoB_2 monolayers, which we focus on the Total Density of States (TDOS) and Projected

Density of States (PDOS) to assess their impact on battery performance.

4.2.2 Band Structure Systems for Monolayer Systems

The electronic properties of two-dimensional materials are pivotal in determining their suitability for various applications. In the case of FeB_2 and MoB_2 monolayers, as well as graphene, the absence of a band gap is indicative of metallic behavior. This characteristic is crucial for applications that require high electrical conductivity, such as electrodes in energy storage devices.

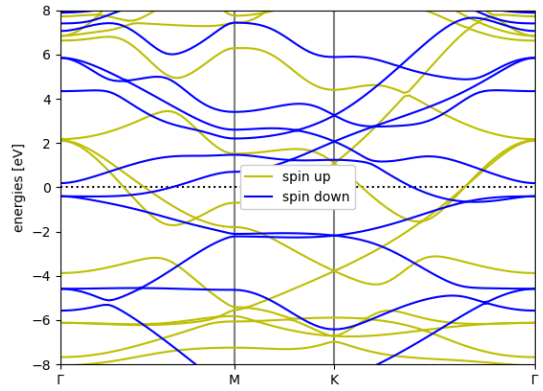

(a) FeB_2

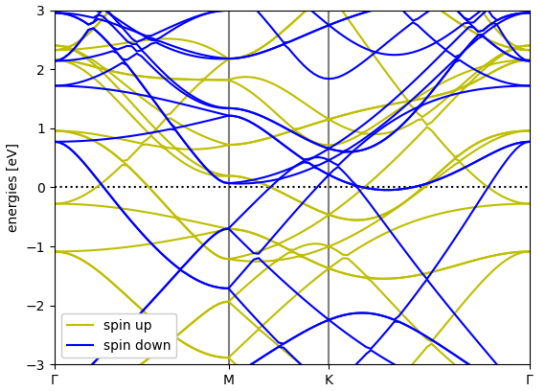

(b) B_2Mo

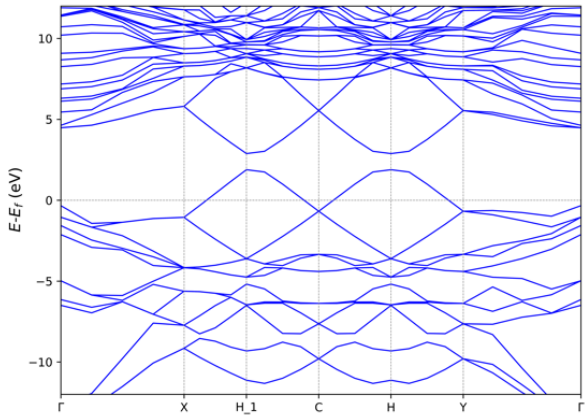

(c) Graphene

Figure 17: The band structure for monolayers. The Fermi level is indicated by the black color broken line at 0 eV.(a) and (b) the GLLBSCM and (c) HSCE06 calculation is employed.

The band structures of FeB_2, MoB_2, and graphene monolayers reveal a significant feature: the absence of a band gap at the Fermi level, marked by the black dashed line at 0 eV. This absence is a clear indication of metallic behavior, which is highly desirable for applications where electrical conductivity is critical. The GLLBSCM and HSCE06 calculations employed in the diagrams further confirm the metallic nature of these materials.

The metallic behavior of these 2D materials, as evidenced by their band structures, makes them excellent candidates for use as electrodes in energy storage devices. Their ability to conduct electricity efficiently can lead to improvements in the performance of batteries and capacitors, which are essential components in the push for renewable energy solutions.

While MoB_2 is well-known for its exceptional electrical properties, the comparison with FeB_2 and graphene monolayers provides valuable insights. All three materials exhibit similar metallic characteristics, yet the subtle differences in their band structures could influence their specific applications. Comprehending these subtleties is vital in customizing materials to fulfill the requirements of diverse high-conductivity applications.

These findings underscore the importance of electronic properties in the selection of materials for technological applications, particularly in the realm of renewable energy where efficiency and conductivity are key. The band structures of FeB_2, MoB_2, and graphene serve as a roadmap for future material design and application development.

4.3 Density state Project and Band structure of Hetero-structure

4.3.1 Total density state and Project Density of States (PDOS) Hetero-structure

We performed Density Functional Theory (DFT) computations and analysis on virgin monolayers of FeB_2 and MoB_2, as well as graphene. These studies are the basic research for understanding the electrical structures of novel 2D heterostructures, which include FeB_2/graphene, MoB_2/graphene, graphene/MoB_2, and graphene/FeB_2. The project densities of states for FeB_2/graphene, MoB_2/graphene graphene/MoB_2, and graphene/FeB_2 hetero- structures.

The PDOS sheds light on the contribution of specific atomic orbitals to the material's electronic properties.

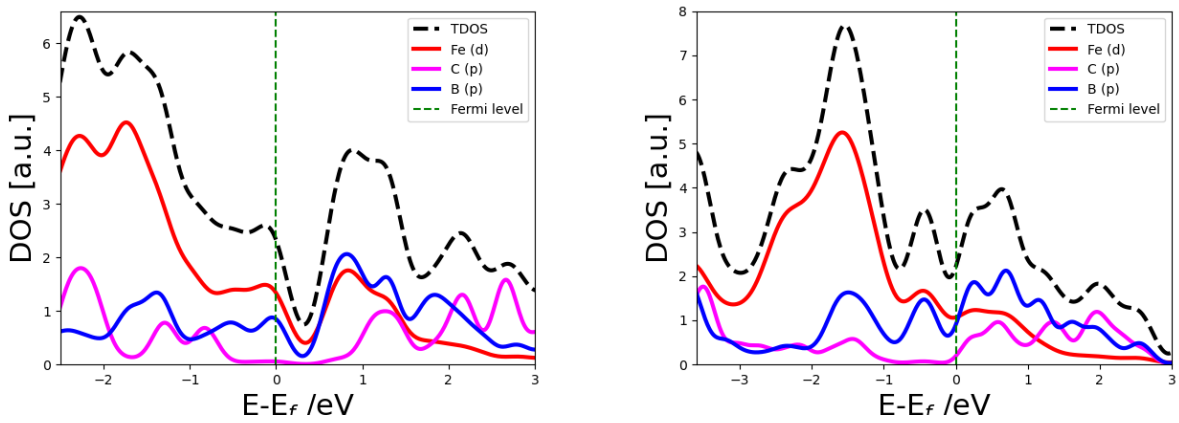

(a) Graphene/FeB_2 (b) B_2Fe/Graphene

Figure 18: The total density of states and project density state for MBene-based heterostructure and the Fermi level is indicated by the black color line at 0 eV. The PBE+D3 calculation is employed.

For graphene/MoB_2, the valence and conduction bands are influenced by the boron (B) atoms' p orbitals , carbon(C) atoms' p orbital and the molybdenum (Mo) atoms' d orbitals. In graphene/FeB_2, the bands are shaped by the boron (B) atoms' p orbitals, carbon (C) atoms' p orbitals and the iron (Fe) atoms' d orbitals.

The DOS plots for these materials show that they have a metallic nature. This is deduced from the fact that the Fermi level, which is the highest energy level occupied by electrons, shifts to 0 eV energy. In metals, the Fermi level lies within the conduction band, allowing for free movement of electrons and hence conductivity.

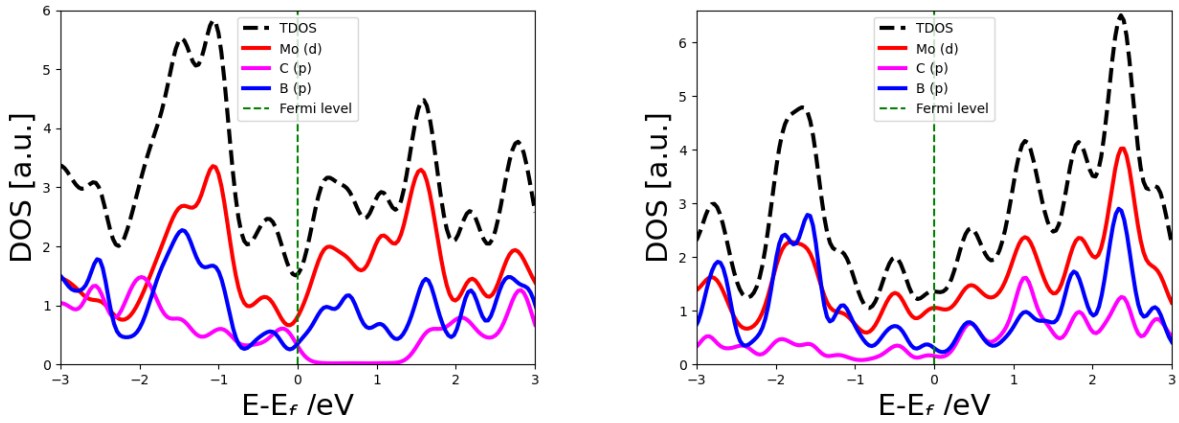

(a) Graphene/MoB_2 (b) B_2Mo/Graphene

Figure 19: The total density of states and project density state for MBene-based hetero-structure and the Fermi level is indicated by the black color line at 0 eV. The PBE+D3 calculation is employed.

4.3.2 Band structure of Hetero-structures of Hetero-structures

The band structure diagrams for graphene/B_2Fe, graphene/B_2Mo, FeB_2/graphene, and MoB_2/graphene monolayers provide significant insights into their electronic properties. The continuous electronic state density at the Fermi level, as indicated by the black broken line at 0 eV, confirms the metallic nature of these MBene-based hetero-structures. This metallic behavior is crucial for applications where high electrical conductivity is desired, such as in electrodes or interconnects in electronic devices.

The location of the valence band maximum (VBM) at the K Point in the Brillouin Zone for these materials suggests that the electrons with the highest energy in the valence band are found at this high-symmetry point. This can have implications for the optical properties of the material, as transitions involving the VBM often contribute to the absorption of light.

On the other hand, the conduction band minimum (CBM) being at the Γ Point indicates that the lowest energy state available to electrons in the conduction band is at the center of the Brillouin Zone, which could affect the material's electrical conductivity and thermal properties.

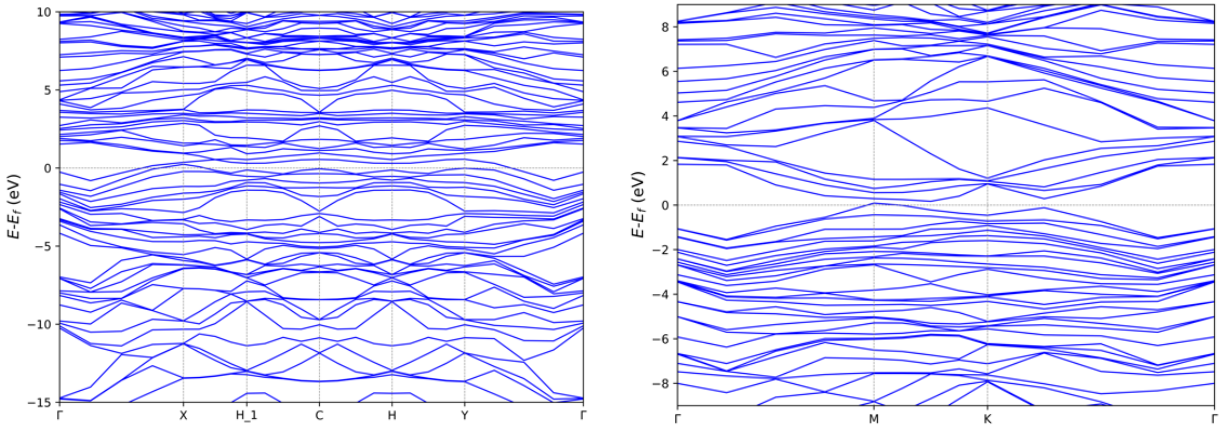

(a) B_2Fe/graphene (b) Graphene/B_2Fe

Figure 20: Band structure of MBene-based hetero-structure. The Fermi level is indicated by the black color Broken line at 0 eV. The HSE06 calculation is employed.

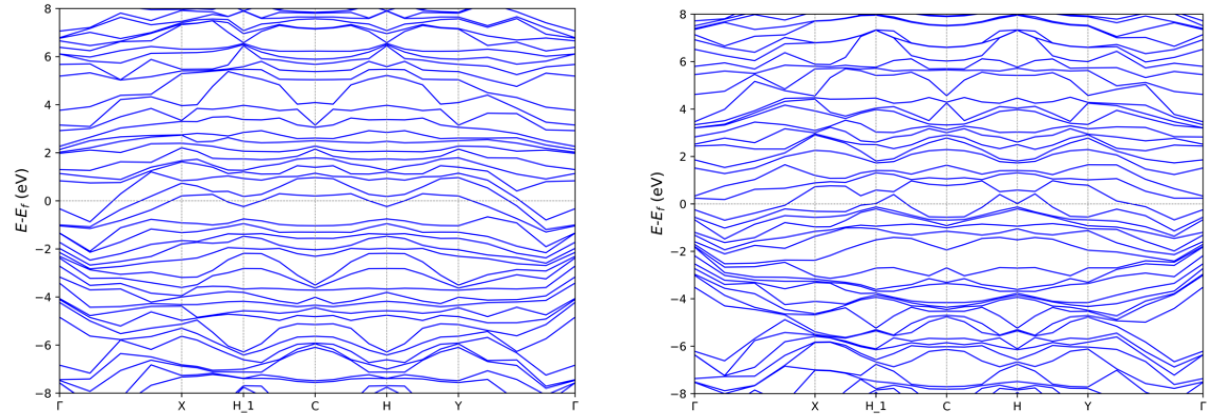

(a) B_2Mo/graphene (b) graphene/B_2Mo

Figure 21: Band structure of MBene-based hetero-structure. The Fermi level is indicated by the black color Broken line at 0 eV. The HSE06 calculation is employed.

The use of the HSE06 calculation method provides a more accurate description of the electronic band structure, especially for materials with strong electronic correlations. This level of precision is necessary to predict the behavior of electrons in these materials accurately and to design devices that can exploit these properties for various technological applications.

Overall, the band structure calculations for these graphene/boride hetero-structures not only confirm their metallic nature but also provide valuable information about their potential

performance in electronic applications. The specific features of the VBM and CBM, along with the detailed band structure provided by the HSE06 calculations, offer a roadmap for further experimental and theoretical investigations into these promising materials.

4.4 Formation Energy for Hetero-structures

We investigated the formation of hetero-structures composed of graphene and two types of MBene materials: MoB_2 and FeB_2 in mono-layer structures. Due to different equilibrium lattice constants of FeB_2 and MoB_2 with graphene, there was a need to reduce the lattice mismatch effect to create the hetero-structures. As a result, the lattice mismatches of graphene or MoB_2 were 2.06% and graphene or FeB_2 were 1.93%, both of which are less than 5%. The lattice mismatch was calculated using equation 3.25. The formation energy (ΔE_{bind}) of graphene/FeB_2, graphene/MoB_2, MoB_2/graphene, and FeB_2/graphene hetero-structures was computed with different exchange correlations and plotted with and without van der Waals corrections at various points as shown in the (Figure 22) below.

We then calculated the formation energy the thermodynamic stability of a hetero-structure material using is determined using equation 3.27 binding(formation) energy (ΔE_{bind}), which represents the energy required to form the hetero-structure from the pristine material. This quantity represents the energy difference between the hetero-structure and the pristine materials. A lower (more negative) formation energy indicates a higher stability of the hetero-structure. We used three different exchange correlation methods to account for the electronic interactions: PBE, optPBE-vdW, and DFT+D3. The latter two methods include van der Waals (vdW) corrections, which are important for describing the weak, long-range interactions between the layers of the hetero-structures. The formation energy of graphene/FeB2 and graphene/MoB_2 hetero-structures were calculated.

We then calculated the formation energy the thermodynamic stability of a hetero-structure material using is determined using equation 3.27 binding(formation) energy (ΔE_{bind}), which

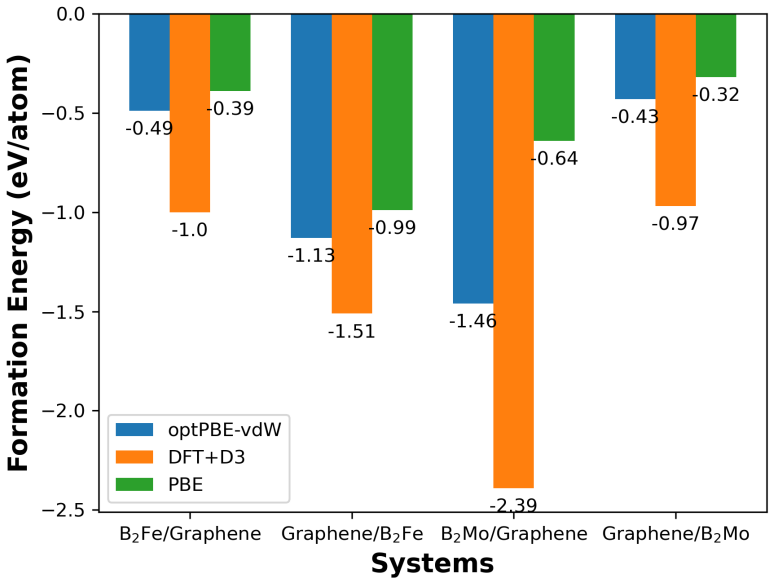

Figure 22: Formation energies for different systems

represents the energy required to form the hetero-structure from the pristine material. This quantity represents the energy difference between the hetero-structure and the pristine materials. A lower (more negative) formation energy indicates a higher stability of the hetero-structure. We used three different exchange correlation methods to account for the electronic interactions: PBE, optPBE-vdW, and DFT+D3. The latter two methods include van der Waals (vdW) corrections, which are important for describing the weak, long-range interactions between the layers of the hetero-structures. The formation energy of graphene/FeB2 and graphene/MoB_2 hetero-structures were calculated.

We plotted the formation energy of four hetero-structures: graphene/MoB_2, MoB_2/graphene, graphene/FeB_2, and FeB_2/graphene, as a function of the interlayer distance. We observed that the formation energy values were more negative with DFT+D3 exchange correlation than with PBE and optPBE-vdW, indicating that vdW corrections enhance the stability of the hetero-structures. We also noticed that the hetero-structures involving FeB_2 had lower formation energy than those involving MoB_2, suggesting that FeB_2 is more compatible with graphene than MoB_2. This result is consistent with the established knowledge of vdW in-

teractions in layered materials, and demonstrates their importance for accurately evaluating the stability of hetero-structures.

When considering PBE and the two van der Waals corrections (optPBE-vdW and DFT+D3), we observed that as the interlayer distance decreased, a repulsive force emerged between the two layers. Conversely, with an increased inter-layer distance, no interaction occurred; however, at a moderate inter-layer distance, attractive forces formed. In our calculations, the HS graphene/MoB_2 interaction was weaker at interlayer distances of 3.499 Å and 3.54 Å, while in the case of HS graphene/FeB_2, the inter-layer distances were 3.343 Å and 3.447 Å. However, for MoB_2/graphene, a much stronger interaction was observed at inter-layer distances of 3.032 Å and 3.187 Å. Surprisingly, the FeB_2/graphene interaction became even more pronounced at interlayer distances of 2.7 Å and 2.75 Å when using DET+D3 and optPBE-vdW, respectively, for different exchange correlations.

4.5 Li atom adsorption on pristine and hetero-structures

Insertion (intercalation) is the reversible introduction of alien species into the gaps between crystals or layers. Layered materials are good hosts for a variety of intercalants, including tiny ions, atoms, and molecules. We computed the adsorption energy of lithium atoms on hetero-structures and pristine MBenes

We chose the best adsorption site by inserting the Li atom in several positions (Figure 23)

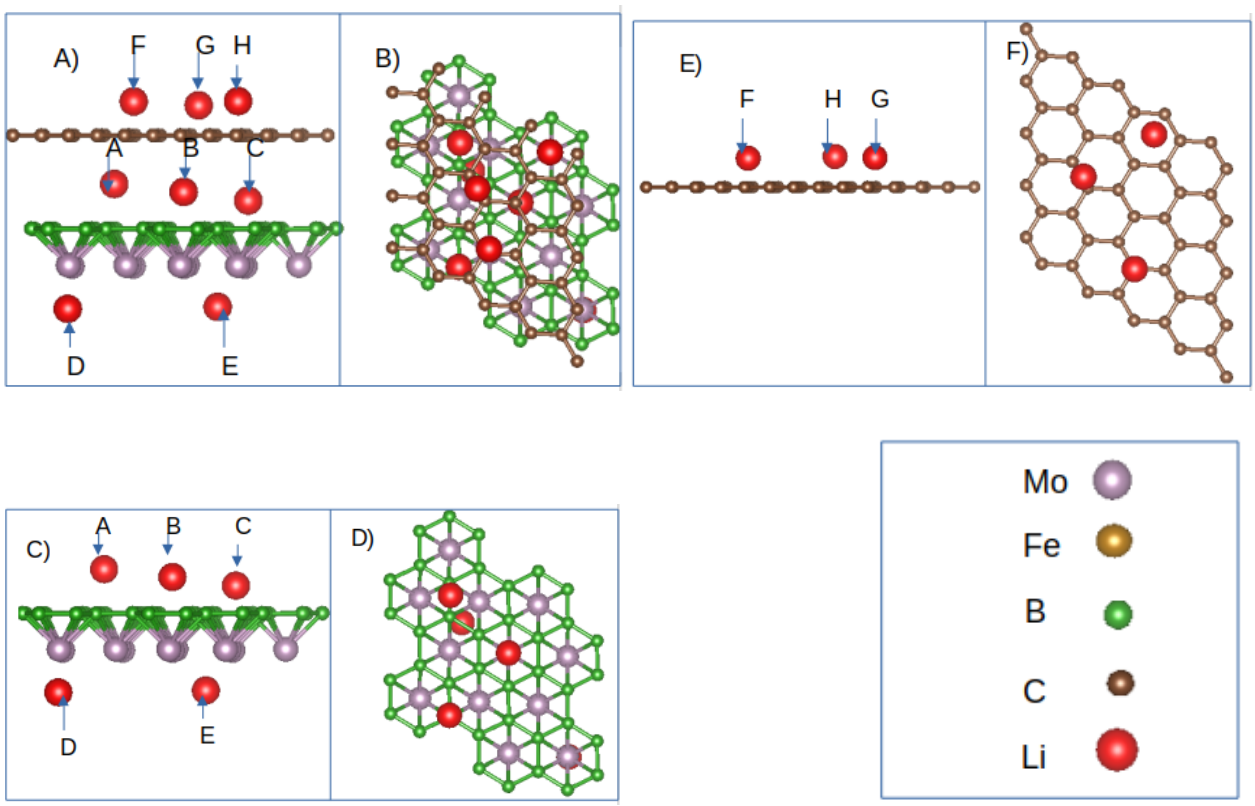

Figure 23: Lithium atom adsorption on hetero-structures and pristine MBenes. A) side view of graphene/MoB_2 of MBene based hetero-structure. B) The top view of graphene/MoB_2 of MBene based hetero-structure. C)side view of MoB_2.D) Top view of MoB_2. E) side view of graphene. F) Top view of graphene.

4.5.1 Adsorption energies of B_2Fe/graphene and graphene/B_2Fe

The heterostructure of B_2Fe/graphene and graphene/B_2Fe is a promising anode material for lithium-ion batteries, as it can enhance the adsorption and diffusion of Li atoms compared to the individual layers of FeB_2 and graphene. In this study, we calculated the adsorption energy of Li atoms on various sites of the heterostructure using different methods, including PBE, OptPBE-vdW, and D3. The results are shown in Table 3, which also includes the adsorption energy of FeB_2 and graphene as references.

Table 3 shows that the adsorption energy of Li atoms on B_2Fe/graphene is more negative than that on graphene/B_2Fe, indicating a stronger interaction between Li and B_2Fe/graphene. This is because the B_2Fe layer can facilitate the charge transfer and electron density between

Li and graphene, increasing their bonding strength. Moreover, the adsorption energy of Li atoms on B_2Fe/graphene is more sensitive to the method and the adsorption site than that on graphene/B_2Fe. For example, the adsorption energy of Li atom on (HCP)B site of B_2Fe/graphene ranges from -1.958 eV (PBE) to -3.154 eV (D3), whereas that on (HCP)B site of graphene/B_2Fe varies from -1.633 eV (PBE) to -2.887 eV (D3). This suggests that the Li-B_2Fe/graphene system requires more dispersion correction than the Li-graphene/B_2Fe system.

The adsorption energy of Li atoms on B_2Fe/graphene and graphene/B_2Fe is also compared to that of FeB_2 and graphene, the two components of the heterostructure. The adsorption energy of Li atoms on B_2Fe/graphene is lower than that of FeB_2, but higher than that of graphene. This means that the B_2Fe/graphene heterostructure has a beneficial effect on Li adsorption, increasing the Li atom's binding strength when compared to the separate layers. This is due to the hybridization of the electronic states of FeB_2 and graphene, which creates new energy levels and enhances charge density at the interface.

Table 3: The calculated adsorption energy with and without dispersion corrections for B_2Fe/graphene and graphene/B_2Fe at various positions.

Sites	B_2Fe/graphene			graphene/B_2Fe			FeB_2
	PBE	OptPBE-vdW	DFT+D3	PBE	OptPBE-vdW	DFT+D3	DFT+D3
(HCP)B	-1.958	-3.141	-3.154	-1.633	-2.777	-2.887	-1.93
(TOP)B	-1.947	-3.153	-3.148	-1.632	-2.775	-2.873	-1.33
(Bridge)B	-1.931	-3.1501	-3.149	-1.629	-2.736	-2.875	-1.36
(Hollow)Fe	-0.817	-1.368	-1.355	-	-	-	-
(Top)Fe	-	-	-0.91	-	-	-0.761	-
(Bridge)C	-	-1.350	0.82	-	-	0.453	-
HPC(C)	-	-	0.52	-	-	0.46	-
Top(C)	-	-	0.85	-	-	0.451	-

The adsorption energy of Li atoms on graphene/B_2Fe is higher than that of FeB_2, but lower than that of graphene. This implies that the graphene/B_2Fe hetero-structure has a detrimental effect on Li adsorption, decreasing the binding strength of Li atoms as compared to the individual layers. This is explained by the fact that the graphene layer acts as a barrier

to charge transfer and electron density between Li and FeB_2, reducing their contact.

The adsorption energy of Li atoms on the hetero-structure is related to the lithium-ion battery performance, as it reflects the thermodynamic stability and the reversibility of the Li insertion and extraction processes. A lower adsorption energy indicates a higher capacity and a lower voltage, while a higher adsorption energy implies a lower capacity and a higher voltage. Therefore, the heterostructure of B_2Fe/graphene and graphene/B_2Fe can offer a trade-off between capacity and voltage, depending on the stacking order and the Li adsorption site. The optimal configuration for the hetero-structure can be determined by further calculating the open-circuit voltage, the theoretical capacity, and the Li diffusion coefficient of the system.

4.5.2 Adsorption energies of The table shows the adsorption energy of Li atoms on graphene/B_2Mo and B_2Mo/graphene

The table shows the adsorption energy of Li atoms on graphene/B_2Mo and B_2Mo/graphene hetero-structures at different sites, calculated by three methods: PBE, OptPBE-vdW, and D3. The adsorption energy of the individual MoB_2 and graphene layers are also given as references. The adsorption energy reflects the stability and affinity of Li atoms on the surface of the materials. A lower (more negative) adsorption energy indicates a stronger binding and a higher capacity for Li storage.

From the table. 4, we can see that the adsorption energy of Li atoms on graphene/B_2Mo is lower than that on B_2Mo/graphene for all the sites and methods, except for the hollow and top Fe sites, where the adsorption energy is very close to zero or slightly positive. This means that Li atoms prefer to adsorb on the B_2Mo side of the hetero-structure, rather than the graphene side. This is consistent with the charge transfer analysis, which shows that Li atoms donate electrons to the B_2Mo layer, creating a strong electrostatic attraction. On the other hand, Li atoms have a weak interaction with the graphene layer, which is nearly charge-neutral.

The table also shows that the adsorption energy of Li atoms on graphene/B_2Mo is lower than that on MoB_2, but higher than that on graphene, for all the sites and methods. This implies that the graphene/B_2Mo hetero-structure has a beneficial effect on Li adsorption, enhancing the binding strength of Li atoms compared to the separate layers. This is due to the hybridization of the electronic states of graphene and MoB_2, which generates new energy levels and increases the charge density at the interface.

The adsorption energy of Li atoms on B_2Mo/graphene is higher than that on MoB_2, but lower than that on graphene, for all the sites and methods. This suggests that the B_2Mo/graphene hetero-structure has an adverse effect on Li adsorption, reducing the binding strength of Li atoms compared to the individual layers. This is explained by the fact that the B_2Mo layer acts as a barrier to charge transfer and electron density between Li and graphene, decreasing their contact. The table also reveals that the adsorption energy of Li atoms on both hetero-

Table 4: The calculated adsorption energy with and without dispersion corrections for graphene/B_2Mo and B_2Mo/graphene at various positions.

Sites	graphene/B_2Mo			B_2Mo/graphene			MoB_2
	PBE	OptPBE-vdW	DFT+D3	PBE	OptPBE-vdW	DFT+D3	DFT+D3
(HCP)B	-1.826	-2.905	-2.912	-1.651	-2.735	-2.908	-1.74
(Top)B	-1.823	-2.893	-2.901	-1.644	-2.731	-2.906	-0.954
(Bridge)B	-1.333	-2.808	-2.348	-1.649	-2.732	-2.905	-0.99
(Hollow)Fe	-	-	-0.56	-0.132	-	-0.215	-
(Top)Fe	-	-	-0.61	-	-	0.796	-
(Bridge)C	-	-	0.56	-	-	1.07	-
HPC(C)	-	-	0.53	-	-	1.11	-
Top(C)	-	-	0.71	-	-	0.86	-

structures is sensitive to the choice of the method and the site. The OptPBE-vdW and D3 methods, which include the dispersion correction, give lower adsorption energies than the PBE method, which neglects the dispersion interaction. This indicates that the dispersion force plays an important role in the Li adsorption on the hetero-structures, especially on the graphene side. The adsorption energy also varies significantly among different sites, depending on the local atomic configuration and coordination.

Generally, the adsorption energy is lower on the B sites than on the Fe or C sites, because the B atoms have a higher electronegativity and a lower coordination number than the Fe or C atoms, making them more attractive and accessible to Li atoms. Among the B sites, the bridge site has the lowest adsorption energy on graphene/B_2Mo, while the HCP site has the lowest adsorption energy on B_2Mo/graphene. This is related to the symmetry and the distance of the B atoms to the adjacent layers.

In summary, the table demonstrates that the graphene/B_2Mo and B_2Mo/graphene heterostructures have different effects on the Li adsorption, depending on the stacking order, the method, and the site. The graphene/B_2Mo heterostructure shows a higher capacity and a stronger stability for Li storage than the B_2Mo/graphene heterostructure, making it a more promising anode material for lithium-ion batteries.

4.6 Effect of Increasing the Concentration of Li-ion

To understand the effect of Li atom adsorption, we investigated the adsorption on the most energetically favorable site HCP(B site) for both graphene/B_2Fe and B_2Mo/graphene heterostructures. The adsorption energy per Li atom for these systems was found to decrease with an increasing number of Li atoms. This trend is depicted in Figure 24(b), where the adsorption energy per Li atom diminishes as the concentration of Li atoms rises. The reduction in adsorption energy per Li atom can be ascribed to the diminished electrostatic interaction between the hetero-structures and Li atoms, which is likely due to increased Li-Li repulsion at higher Li atom concentrations.

For the graphene/B_2Fe hetero-structure, the adsorption energy decreased from -2.887 eV for a single Li atom to -0.901 eV for three Li atoms. Similarly, for the graphene/B_2Mo hetero-structure, the adsorption energy decreased from -2.912 eV for one Li atom to -0.718 eV for three Li atoms. The B_2Fe/graphene hetero-structure showed a decrease in adsorption energy from -3.154 eV to -0.746 eV, and the B_2Mo/graphene hetero-structure from -2.908

eV to -0.408 eV as the number of Li atoms increased from one to three.

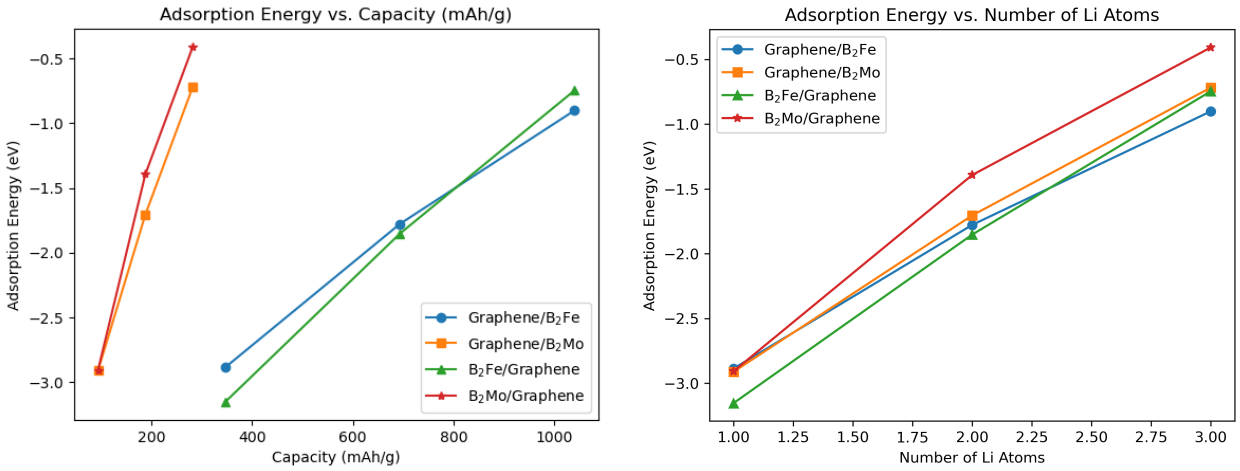

(a) . (b) .

Figure 24: Adsorption energies as function of number of Li atoms (a) adsorbing more than one Li atoms at most energetic site and adsorption energies as functions of capacity (mAh/g) (b) for B_2Mo/graphene, graphene/B_2Mo, B_2Fe/graphene and graphene/B_2Fe hetero- structures.

4.7 Electrochemical Properties

4.7.1 Open-Circuit-Voltage (OCV)

To determine the electrochemical properties of the Li absorption process into both hetero-structures, the open-circuit voltage (OCV) was calculated (using equation 3.29) and the performance of the rechargeable lithium batteries was indicated by the OCV values. We only consider the most stable adsorption sites for both hetero-structures at the most negative adsorption energy. The largest adsorption energy for Li atom adsorption is the highest voltage.

To determine the electrochemical properties of the Li adsorption process into the graphene/FeB_2 and graphene/MoB_2 hetero-structures, the Open-circuit voltage (OCV) were calculated.

To evaluate the electrochemical properties of lithium (Li) atom adsorption on various hetero-structures, our investigation centered on the open-circuit voltage (OCV). OCV is a pivotal

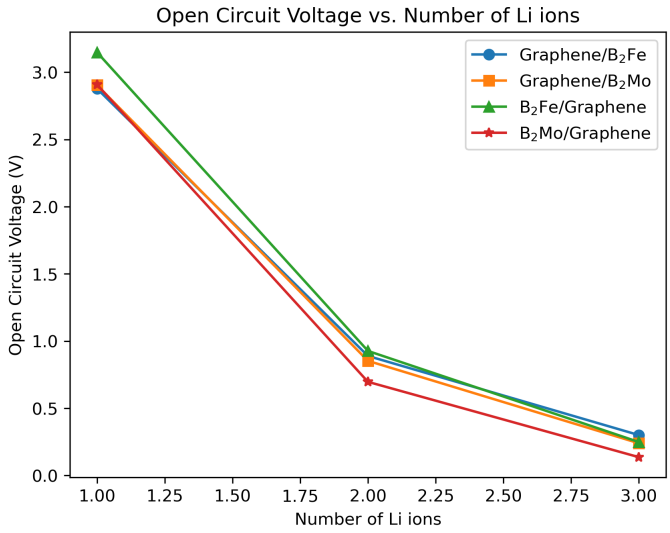

Figure 25: Calculated open circuit voltage (OCV) for Li atom adsorption as a function of number of Li ions.

metric that reflects the potential performance of rechargeable lithium batteries. The determination of OCV values was anchored in identifying the most stable adsorption sites, which are characterized by the lowest adsorption energy.

Upon examining the OCV trends, we observed a consistent decrease as the number of Li atoms adsorbed on the hetero-structures increased. This pattern mirrors the behavior seen in analogous systems, such as MoS_2/graphene[147], MoS_2/Ti_2CT_2, [148], and MoS_2/Ti_3CO_2 [149]. The underlying cause of this OCV reduction is twofold: the ion-ion interactions among the Li atoms themselves, and the comparatively modest electrostatic attraction between the Li ions and the hetero-structures.

For the Graphene/B_2Fe hetero-structure, the OCV values exhibited a decline from 2.887 V to 0.901 V. Similarly, the graphene/B_2Mo hetero-structure showed a decrease from 2.912 V to 0.718 V as the Li atom count rose from one to three as show figure 25. In the case of B_2Fe/graphene, the OCV diminished from 3.154 V to 0.746 V, and for B_2Mo/graphene, it fell from 2.908 V to 0.408 V.

Despite this decrease, all hetero-structures maintained positive OCV values, signifying the

chemical stability of Li adsorption within the graphene/B_2Fe, B_2Fe/graphene, B_2Mo/graphene, and graphene/B_2Mo configurations. The final positive voltages 0.901 V, 0.746 V, 0.408 V, and 0.718 V for Graphene/B_2Fe, B_2Fe/Graphene, B_2Mo/Graphene, and Graphene/B_2Mo, respectively—indicate high energy densities, which are advantageous for Li-ion batteries.

Furthermore, the OCVs for these hetero-structures fall within the optimal range of 0.2 to 1 V[150] VS_2 /Ti_2 CT_2, suggesting their potential as promising anode materials for Li-ion batteries. The voltage range between 0.2 and 3V is deemed suitable for anode materials as it not only promotes high energy density but also helps prevent the formation of lithium clusters. Our analysis plays a crucial role in ref-ining the design of anode materials, aiming to enhance the capacities and overall performance of lithium-ion batteries.

4.7.2 Theoretical Capacity

These negative adsorption energies indicate that Li adsorption is energetically favorable and becomes more stable as the number of Li atoms increases in both graphene/B_2Fe and B_2Mo/graphene hetero-structures. Figure 24(a) illustrates the adsorption energies of both hetero-structures as functions of specific capacity, which is determined by the quantity of Li atoms adsorbed on the material. The specific capacities for the graphene/B_2Fe and B_2Fe/graphene hetero-structures are 346.7 mAh/g, 693.4 mAh/g, and 1040.1 mAh/g for one, two, and three Li atoms, respectively. similarly For the graphene/B_2Mo and B_2Mo/graphene heteros-tructures the corresponding number of Li atoms ase show the figure 26

This analysis underscores the potential of these hetero-structures as anode materials in Li-ion batteries, with their capacity to adsorb Li atoms being a key factor in their performance. The stability of Li adsorption suggests that these materials could be promising candidates for high-capacity anode materials in next-generation batteries.

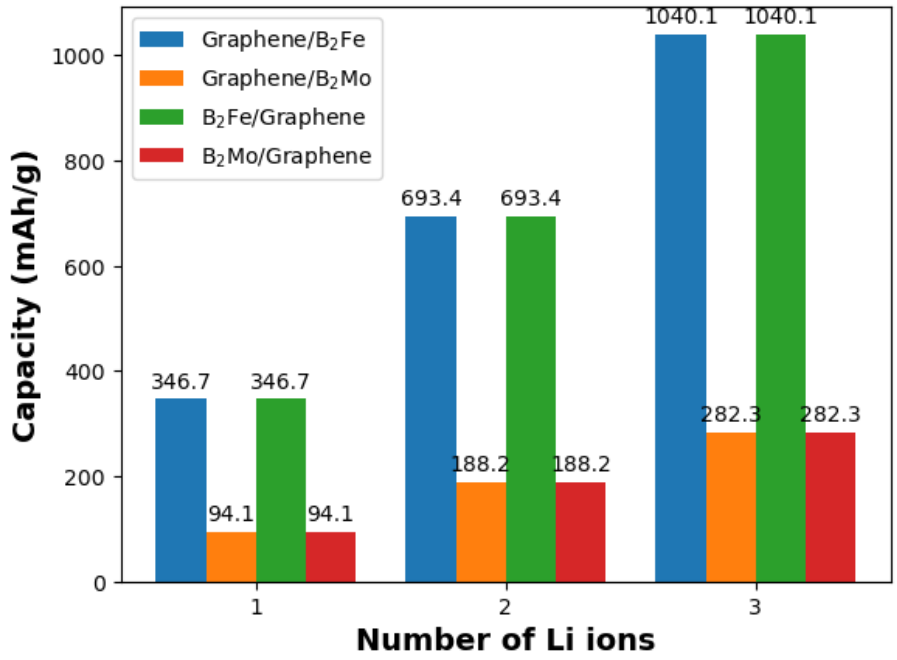

Figure 26: Calculated capacity(mAh/g) for B_2Mo/graphene, graphene/B_2Mo , B2Fe/graphene, and graphene/B_2Fe hetero-structures. MBene-based hetero-structures.

4.8 Li-ion diffusion of Hetero-strucure

In lithium intercalation batteries, the kinetics of lithium extraction and reinsertion into the host structures of the electrode materials are critical. For FeB_2 and MoB_2 anode materials, the intercalation rate may be hindered by either electrical or ionic conductivities. This section examines the mobility of lithium ions within the intercalation hosts, with a particular focus on the role of Density Functional Theory (DFT) in evaluating this process. DFT is not only pivotal for energy calculations and structural optimization but also for investigating lithium ion transport within the crystal structure.

The Climbing Image Nudged Elastic Band (CI-NEB) method within the DFT+D3 framework was employed to study Li diffusion in lithiated and delithiated systems and to calculate the corresponding activation energies. The CI-NEB images were relaxed without volume and cell parameter relaxation and converged when the residual force fell below 0.05 eV/Å. This method was used to identify all feasible lithium-ion migration pathways with open space and

short hopping distances, and to calculate the migration energy barriers.

The structures were first created by introducing a single lithium ion to the hetero-structures out of nine Li sites (graphene/B_2Fe, B_2Fe/graphene, graphene/B_2Mo, and B_2Mo/graphene) and calculating the Li diffusion activation barriers in different lithium-rich phases. Five intermediates were constructed to interpolate the diffusion path between the initial and final states in each direction.

The two-dimensional Li^+ transport pathways are summarized in the figure and table provided. The calculated high energy barriers for graphene/B_2Mo ($E_b \approx 0.073$ eV and 0.063 eV) indicate better performance compared to graphene/B_2Fe ($E_b = 0.064$ eV and 0.085 eV), B_2Fe/graphene ($E_b = 0.040$ eV and 0.057 eV), and B_2Mo/graphene ($E_b = 0.043$ eV and 0.075 eV) along the (001) plane.

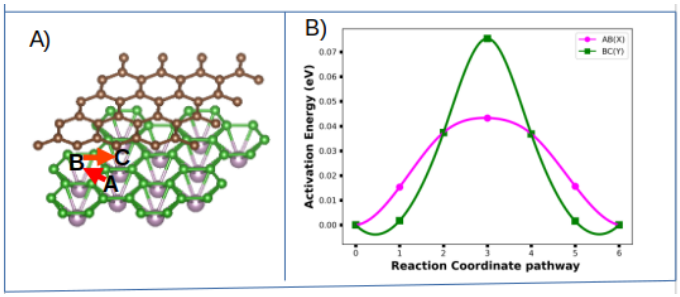

Figure 27: pathways for Li^+ and Li^+ surface diffusion in graphene/B_2Mo.

The study's findings reveal distinct differences in diffusion rates and coefficients across various materials at a temperature of 300 K. For graphene/B_2Mo, the diffusion rate along the AB(x) path was 5.94×10^{11} s^{-1}, with a corresponding diffusion coefficient of 3.86×10^{-8} m^2/s. Conversely, along the BC(Y) path, these values increased to 8.74×10^{11} s^{-1} and 1.09×10^{-7} m^2/s, respectively, indicating a more efficient diffusion along the BC(Y) path for this material.

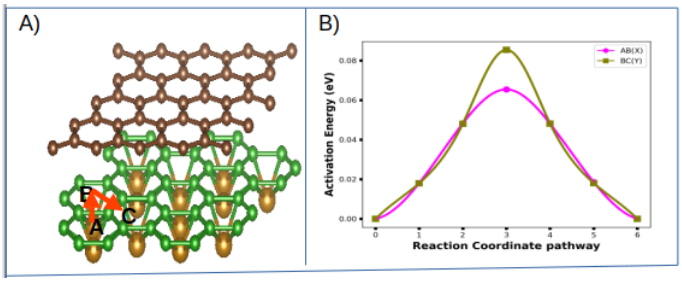

Figure 28: pathways for Li^+ and Li^+ surface diffusion in graphene/B_2Fe.

graphene/B_2Fe showed a higher diffusion rate of 8.74×10^{11} s^{-1} along the AB(x) path compared to 3.73×10^{11} s^{-1} along the BC(Y) path. However, the diffusion coefficient was lower along the AB(x) path (8.32×10^{-8} m^2/s) than the BC(Y) path (6.48×10^{-8} m^2/s), suggesting a complex interplay between the diffusion rate and the diffusion coefficient.

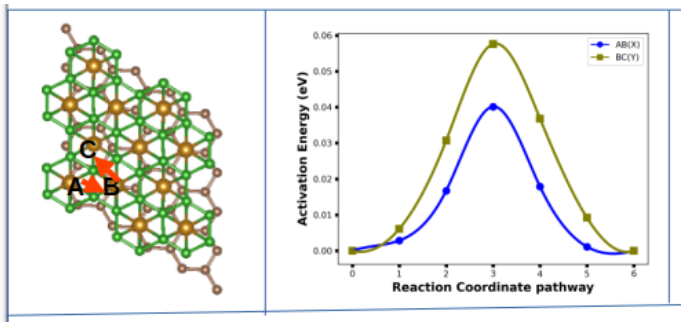

Figure 29: pathways for Li^+ and Li^+ surface diffusion in B_2Fe/graphene.

For B_2Fe/graphene, the highest diffusion rate observed was 2.13×10^{12} s^{-1} along the AB(x) path, with a diffusion coefficient of 2.34×10^{-7} m^2/s, denoting a highly efficient diffusion process. The BC(Y) path showed a lower rate and coefficient, 1.10×10^{12} s^{-1} and 1.78×10^{-7} m^2/s, respectively.

Lastly, B_2Mo/graphene exhibited a diffusion rate of 1.89×10^{12} s^{-1} along the AB(x) path and a slightly lower rate of 5.49×10^{11} s^{-1} along the BC(Y) path. The diffusion coefficients were 1.23×10^{-7} m^2/s and 3.51×10^{-8} m^2/s, respectively, which is consistent with the trend of higher diffusion rates correlating with higher diffusion coefficients.

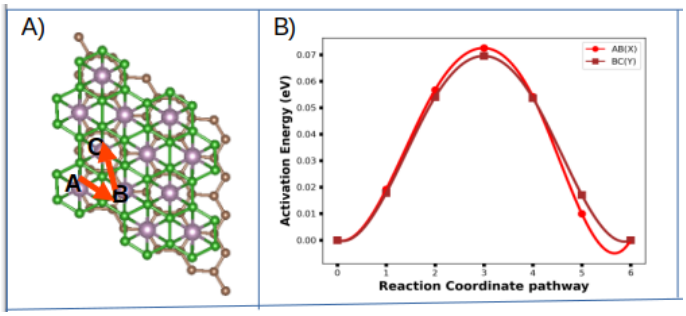

Figure 30: pathways for Li^+ and Li^+ surface diffusion in B_2Mo/graphene.

Table 5: Diffusion rate (r) and diffusion coefficient (D) for various materials hetero-structures at 300 K.

Materials	Path	E_b (eV)	a (Å)	Diffusion Rate r (s^{-1})	Diffusion Coefficient D (m^2/s)
Graphene/B_2Mo	AB(x)	0.073	2.548	5.94×10^{11}	3.86×10^{-8}
	BC(Y)	0.063	3.55	8.74×10^{11}	1.09×10^{-7}
Graphene/B_2Fe	AB(x)	0.064	3.086	8.74×10^{11}	8.32×10^{-8}
	BC(Y)	0.085	4.167	3.73×10^{11}	6.48×10^{-8}
B_2Fe/Graphene	AB(x)	0.040	3.456	2.13×10^{12}	2.34×10^{-7}
	BC(Y)	0.057	4.023	1.10×10^{12}	1.78×10^{-7}
B_2Mo/Graphene	AB(x)	0.043	2.551	1.89×10^{12}	1.23×10^{-7}
	BC(Y)	0.075	2.528	5.49×10^{11}	3.51×10^{-8}

These results underscore the critical role of material composition and structural pathways in dictating the efficiency of diffusion processes at the atomic scale. The data clearly indicates that diffusion characteristics are highly material-specific and path-dependent, which could have substantial implications for the design and application of these materials in various technological domains.

CHAPTER 5

CONCLUSION

We have carried out DFT studies to study MBene-based hetero-structures for lithium-ion battery anodes has yielded significant insights into their structural and electrochemical properties. The simulations of B_2Fe/graphene and B_2Mo/graphene, as well as the pristine materials, have established optimal lattice constants and minimal lattice mismatches, indicating a high degree of structural compatibility and potential for robust performance. The binding and adsorption energies, particularly when considering van der Waals forces within the DFT+D3 framework, reinforce the stability and integrity of these hetero-structures.

The Li adsorption energy was found to decrease with more Li ions at the (HCP) B site, and the electrostatic interaction between Li ions diminished as Li-Li repulsion increased with Li-ion concentration. The Open Circuit Voltage (OCV) for MBene-based hetero-structures ranged from 0.2 to 3 V, and the theoretical capacities for Graphene B_2Fe and B_2Mo/Graphene were -693.4 mAh/g and -1040.1 mAh/g, respectively. All of the hetero-structures showed promise as anode materials for rechargeable lithium batteries due to their favorable electrochemical properties.

The electrical and ionic conductivities, which are critical to the performance of lithium intercalation, have been thoroughly examined. The application of the CI-NEB method within the DFT+D3 framework has allowed for precise determination of the activation energies for Li diffusion, shedding light on the mobility of lithium ions within the electrode materials. The calculated diffusion rates and coefficients, derived from the activation energy for each

diffusion path, offer a quantitative measure of the efficiency of lithium transport within these hetero-structures. Notably, graphene/B_2Mo stands out with its lower energy barriers, indicating enhanced performance along the (001) plane.

Moreover, the hetero-structures' potential as anode materials is further supported by their favorable electrochemical properties, such as the range of open circuit voltages and the substantial theoretical capacities. These properties, coupled with the detailed analysis of lithium ion mobility and the implications for battery design, underscore the hetero-structures' suitability for use in rechargeable lithium batteries. The implications for battery design are significant, highlighting the importance of material composition and diffusion pathways in achieving efficient lithium intercalation.

RECOMMENDATION

For future research, it is recommended to extend the investigation of MBene-based hetero-structures, specifically B_2Fe/Graphene and B_2Mo/Graphene, utilizing advanced computational tools such as VASP and Gpaw. These platforms offer a robust framework for density functional theory (DFT) simulations, which can provide deeper insights into the material properties and electrochemical behaviors of these hetero-structures.

Further studies should consider the application of these hetero-structures in a broader range of battery technologies beyond lithium-ion, including lithium-sulfur (Li-S) and batteries utilizing alternative cations such as Mg^{2+}, Na^{+}, Al^{3+}, and Ca^{2+}. The exploration of these materials in different battery systems may reveal versatile performance and adaptability, potentially leading to breakthroughs in energy storage solutions.

Additionally, it is crucial to integrate theoretical material engineering with experimental validation to comprehensively understand the structure and evaluate the electrode performance of these hetero-structures. Such collaborative efforts between computational predictions and practical experiments will enhance the reliability of the findings and accelerate the development of high-performance batteries. This holistic approach will not only validate the computational models but also guide the design of next-generation battery materials.

REFERENCES

[1] W. S. V. Lee, T. Xiong, X. Wang, and J. Xue, "Unraveling mos2 and transition metal dichalcogenides as functional zinc-ion battery cathode: A perspective," *Small Methods*, vol. 5, no. 1, p. 2000815, 2021.

[2] F. Chen, Q. Tang, T. Ma, B. Zhu, L. Wang, C. He, X. Luo, S. Cao, L. Ma, and C. Cheng, "Structures, properties, and challenges of emerging 2d materials in bioelectronics and biosensors," *InfoMat*, vol. 4, no. 5, p. e12299, 2022.

[3] V. G. Nair, M. Birowska, D. Bury, M. Jakubczak, A. Rosenkranz, and A. M. Jastrzebska, "2d mbenes: a novel member in the flatland," *Advanced Materials*, vol. 34, no. 23, p. 2108840, 2022.

[4] C. Liu, Z. G. Neale, and G. Cao, "Understanding electrochemical potentials of cathode materials in rechargeable batteries," *Materials Today*, vol. 19, no. 2, pp. 109–123, 2016.

[5] H. Gunda, L. E. Klebanoff, P. A. Sharma, A. K. Varma, V. Dolia, K. Jasuja, and V. Stavila, "Progress, challenges, and opportunities in the synthesis, characterization, and application of metal-boride-derived two-dimensional nanostructures," *ACS Materials Letters*, vol. 3, no. 5, pp. 535–556, 2021.

[6] M. Khazaei, J. Wang, M. Estili, A. Ranjbar, S. Suehara, M. Arai, K. Esfarjani, and S. Yunoki, "Novel mab phases and insights into their exfoliation into 2d mbenes," *Nanoscale*, vol. 11, no. 23, pp. 11 305–11 314, 2019.

[7] A. Sharma, V. Rangra, and A. Thakur, "Synthesis, properties, and applications of mbenes (two-dimensional metal borides) as emerging 2d materials: a review," *Journal of Materials Science*, vol. 57, no. 27, pp. 12 738–12 751, 2022.

[8] A. Hayat, T. Bashir, A. M. Ahmed, Z. Ajmal, M. M. Alghamdi, A. A. El-Zahhar, M. Sohail, M. A. Amin, Y. Al-Hadeethi, E. Ghasali *et al.*, "Novel 2d mbenes-synthesis, structure, properties with excellent performance in energy conversion and storage: A review," *Materials Science and Engineering: R: Reports*, vol. 159, p. 100796, 2024.

[9] E. Johansson, "Theoretical studies of the coupling between electronic, vibrational, configurational and structural effects in metal borides," Ph.D. dissertation, Linköping University Electronic Press, 2021.

[10] J. P. Perdew and K. Schmidt, "Jacob's ladder of density functional approximations for the exchange-correlation energy," in *AIP Conference Proceedings*, vol. 577, no. 1. American Institute of Physics, 2001, pp. 1–20.

[11] L. Agosta, F. Gala, and G. Zollo, "Water diffusion on tio2 anatase surface," in *AIP Conference Proceedings*, vol. 1667, no. 1. AIP Publishing, 2015.

[12] P. Panigrahi, *Controlling electronic and magnetic properties of ultra narrow multilayered nanowires*. Michigan Technological University, 2009.

[13] J. Hafner and G. Kresse, "The vienna ab-initio simulation program vasp: An efficient and versatile tool for studying the structural, dynamic, and electronic properties of materials," in *Properties of Complex Inorganic Solids*. Springer, 1997, pp. 69–82.

[14] S. Carley, X. Gao, L. V. White, J. A. Engel-Cox, J. A. Engel-Cox, and A. Chapman, "Open access edited by," *Insights in Energy and Society: 2022*, p. 35, 2023.

[15] P. Smith, H. Haberl, A. Popp, K.-h. Erb, C. Lauk, R. Harper, F. N. Tubiello, A. de Siqueira Pinto, M. Jafari, S. Sohi *et al.*, "How much land-based greenhouse gas mitigation can be achieved without compromising food security and environmental goals?" *Global change biology*, vol. 19, no. 8, pp. 2285–2302, 2013.

[16] F. Tanko, "Analysis of common issues in global energy production, consumption and emission pathways in the bp, iea 2021 weo and paris agreement," *Consumption and Emission Pathways in the BP, IEA*, 2021.

[17] V. Dusastre and L. Martiradonna, "Materials for sustainable energy," *Nature Materials*, vol. 16, no. 1, pp. 15–15, 2017.

[18] H. G. Kim and H.-B.-R. Lee, "Atomic layer deposition on 2d materials," *Chemistry of Materials*, vol. 29, no. 9, pp. 3809–3826, 2017.

[19] Y. Ma, S. Kolekar, H. Coy Diaz, J. Aprojanz, I. Miccoli, C. Tegenkamp, and M. Batzill, "Metallic twin grain boundaries embedded in mose2 monolayers grown by molecular beam epitaxy," *ACS nano*, vol. 11, no. 5, pp. 5130–5139, 2017.

[20] M. Liang and L. Zhi, "Graphene-based electrode materials for rechargeable lithium batteries," *Journal of Materials Chemistry*, vol. 19, no. 33, pp. 5871–5878, 2009.

[21] M. Mortazavi, C. Wang, J. Deng, V. B. Shenoy, and N. V. Medhekar, "Ab initio characterization of layered mos2 as anode for sodium-ion batteries," *Journal of Power Sources*, vol. 268, pp. 279–286, 2014.

[22] Y. Jing, Z. Zhou, C. R. Cabrera, and Z. Chen, "Metallic vs2 monolayer: a promising 2d anode material for lithium ion batteries," *The Journal of Physical Chemistry C*, vol. 117, no. 48, pp. 25 409–25 413, 2013.

[23] R. Zhang, X. Wu, and J. Yang, "Blockage of ultrafast and directional diffusion of li atoms on phosphorene with intrinsic defects," *Nanoscale*, vol. 8, no. 7, pp. 4001–4006, 2016.

[24] W. Li, Y. Yang, G. Zhang, and Y.-W. Zhang, "Ultrafast and directional diffusion of lithium in phosphorene for high-performance lithium-ion battery," *Nano letters*, vol. 15, no. 3, pp. 1691–1697, 2015.

[25] P. Liang, Y. Cao, B. Tai, L. Zhang, H. Shu, F. Li, D. Chao, and X. Du, "Is borophene a suitable anode material for sodium ion battery?" *Journal of Alloys and Compounds*, vol. 704, pp. 152–159, 2017.

[26] G. A. Tritsaris, E. Kaxiras, S. Meng, and E. Wang, "Adsorption and diffusion of lithium on layered silicon for li-ion storage," *Nano letters*, vol. 13, no. 5, pp. 2258–2263, 2013.

[27] N. K. Jena, R. B. Araujo, V. Shukla, and R. Ahuja, "Borophane as a benchmate of graphene: a potential 2d material for anode of li and na-ion batteries," *ACS applied materials & interfaces*, vol. 9, no. 19, pp. 16 148–16 158, 2017.

[28] H. Jiang, W. Shyy, M. Liu, L. Wei, M. Wu, and T. Zhao, "Boron phosphide monolayer as a potential anode material for alkali metal-based batteries," *Journal of Materials Chemistry A*, vol. 5, no. 2, pp. 672–679, 2017.

[29] Q. Sun, Y. Dai, Y. Ma, T. Jing, W. Wei, and B. Huang, "Ab initio prediction and characterization of mo2c monolayer as anodes for lithium-ion and sodium-ion batteries," *The journal of physical chemistry letters*, vol. 7, no. 6, pp. 937–943, 2016.

[30] D. Sun, M. Wang, Z. Li, G. Fan, L.-Z. Fan, and A. Zhou, "Two-dimensional ti3c2 as anode material for li-ion batteries," *Electrochemistry communications*, vol. 47, pp. 80–83, 2014.

[31] D. H. Ho, Y. Y. Choi, S. B. Jo, J.-M. Myoung, and J. H. Cho, "Sensing with mxenes: progress and prospects," *Advanced Materials*, vol. 33, no. 47, p. 2005846, 2021.

[32] B. Zhang, J. Zhou, and Z. Sun, "Mbenes: progress, challenges and future," *Journal of Materials Chemistry A*, vol. 10, no. 30, pp. 15 865–15 880, 2022.

[33] A. Bano, D. K. Pandey, A. Modi, and N. Gaur, "Mob 2 driven metallic behavior and interfacial charge transport mechanism in mos 2/mob 2 heterostructure: A first-principles study," *Scientific Reports*, vol. 8, no. 1, p. 14444, 2018.

[34] F. Li and Q. Tang, "First-principles calculations of tib mbene monolayers for hydrogen evolution," *ACS Applied Nano Materials*, vol. 2, no. 11, pp. 7220–7229, 2019.

[35] F. Wei, S. Xu, J. Li, S. Yuan, B. Jia, S. Gao, G. Liu, and P. Lu, "Computational investigation of two-dimensional vanadium boride compounds for na-ion batteries," *ACS omega*, vol. 7, no. 17, pp. 14 765–14 771, 2022.

[36] S. Luo, J. Zhao, Y. Wang, Y. Zhang, Y. Xiong, N. Ma, and J. Fan, "First-principles study of feb2 monolayers as high-capacity electrode materials for mg-ion batteries," *The Journal of Physical Chemistry C*, 2023.

[37] T. Xu, Y. Wang, Z. Xiong, Y. Wang, Y. Zhou, and X. Li, "A rising 2d star: novel mbenes with excellent performance in energy conversion and storage," *Nano-Micro Letters*, vol. 15, no. 1, p. 6, 2023.

[38] N. Qin, S.-Y. Liu, Z. Li, H. Zhao, and S. Wang, "First-principles studies for the stability of a graphene-like boron layer on crb2 (0001) and mob2 (0001)," *Journal of Physics: Condensed Matter*, vol. 23, no. 22, p. 225501, 2011.

[39] C. Wang, C. Yang, and Z. Zheng, "Toward practical high-energy and high-power lithium battery anodes: present and future," *Advanced Science*, vol. 9, no. 9, p. 2105213, 2022.

[40] L. Miao, J. Zhang, Y. Lv, L. Gan, and M. Liu, "Dendrite-free engineering toward efficient zinc storage: Recent progress and future perspectives," *Chemistry–A European Journal*, vol. 29, no. 20, p. e202203973, 2023.

[41] S. Pakhira, K. P. Lucht, and J. L. Mendoza-Cortes, "Dirac cone in two dimensional bilayer graphene by intercalation with v, nb, and ta transition metals," *The Journal of chemical physics*, vol. 148, no. 6, 2018.

[42] J. Hui, N. B. Schorr, S. Pakhira, Z. Qu, J. L. Mendoza-Cortes, and J. Rodríguez-López, "Achieving fast and efficient k+ intercalation on ultrathin graphene electrodes modified by a li+ based solid-electrolyte interphase," *Journal of the American Chemical Society*, vol. 140, no. 42, pp. 13 599–13 603, 2018.

[43] R. Mas-Balleste, C. Gomez-Navarro, J. Gomez-Herrero, and F. Zamora, "2d materials: to graphene and beyond," *Nanoscale*, vol. 3, no. 1, pp. 20–30, 2011.

[44] J. Bi, Z. Du, J. Sun, Y. Liu, K. Wang, H. Du, W. Ai, and W. Huang, "On the road to the frontiers of lithium-ion batteries: A review and outlook of graphene anodes," *Advanced Materials*, vol. 35, no. 16, p. 2210734, 2023.

[45] Y. Dong, Z.-S. Wu, W. Ren, H.-M. Cheng, and X. Bao, "Graphene: a promising 2d material for electrochemical energy storage," *Science Bulletin*, vol. 62, no. 10, pp. 724–740, 2017.

[46] W. Deng, X. Zhou, Q. Fang, and Z. Liu, "Microscale lithium metal stored inside cellular graphene scaffold toward advanced metallic lithium anodes," *Advanced Energy Materials*, vol. 8, no. 12, p. 1703152, 2018.

[47] E. Muchuweni, E. T. Mombeshora, C. M. Muiva, and T. S. Sathiaraj, "Lithium-ion batteries: Recent progress in improving the cycling and rate performances of transition metal oxide anodes by incorporating graphene-based materials," *Journal of Energy Storage*, vol. 73, p. 109013, 2023.

[48] N. Verma, P. Jamdagni, A. Kumar, S. Srivastava, and K. Tankeshwar, "Recent advances in 2d anode materials for na-ion batteries from a theoretical perspective," *Critical Reviews in Solid State and Materials Sciences*, pp. 1–42, 2023.

[49] J. Jia, B. Li, S. Duan, Z. Cui, and H. Gao, "Monolayer mbenes: prediction of anode materials for high-performance lithium/sodium ion batteries," *Nanoscale*, vol. 11, no. 42, pp. 20 307–20 314, 2019.

[50] S. Ma, H. Zhang, Z. Cheng, X. Xie, X. Zhang, G. Liu, and G. Chen, "A novel tetrahex-carbon as a high-performance anode material for na-ion and k-ion batteries," *Colloids and Surfaces A: Physicochemical and Engineering Aspects*, p. 133092, 2023.

[51] J. B. Goodenough and K.-S. Park, "The li-ion rechargeable battery: a perspective," *Journal of the American Chemical Society*, vol. 135, no. 4, pp. 1167–1176, 2013.

[52] M. Winter, J. O. Besenhard, M. E. Spahr, and P. Novak, "Insertion electrode materials for rechargeable lithium batteries," *Advanced materials*, vol. 10, no. 10, pp. 725–763, 1998.

[53] S. Zhu, J. Han, Y.-N. Wang, T.-S. Pan, Y.-M. Wei, W.-L. Song, H.-S. Chen, and D. Fang, "In-situ heat generation measurement of the anode and cathode in a single-layer lithium ion battery cell," *International Journal of Energy Research*, vol. 44, no. 11, pp. 9141–9148, 2020.

[54] M. Z. Jacobson, *100% clean, renewable energy and storage for everything*. Cambridge University Press, 2020.

[55] R. Jain, *Next-Generation Anode Materials for Metal-Ion Batteries*. Rensselaer Polytechnic Institute, 2021.

[56] N. Pradeep, E. Sivasenthil, B. Janarthanan, and S. Sharmila, "A review of anode material for lithium ion batteries," in *Journal of Physics: Conference Series*, vol. 1362, no. 1. IOP Publishing, 2019, p. 012026.

[57] J. Niu and S. Kang, "New high-energy anode materials," 2019.

[58] M. S. Whittingham, "History, evolution, and future status of energy storage," *Proceedings of the IEEE*, vol. 100, no. Special Centennial Issue, pp. 1518–1534, 2012.

[59] W. Xu, J. Wang, F. Ding, X. Chen, E. Nasybulin, Y. Zhang, and J.-G. Zhang, "Lithium metal anodes for rechargeable batteries," *Energy & Environmental Science*, vol. 7, no. 2, pp. 513–537, 2014.

[60] D. Wu, X. Han, C. Wu, Y. Song, J. Li, Y. Wan, X. Wu, and X. Tian, "Two-dimensional transition metal boron cluster compounds (mb n enes) with strain-independent room-temperature magnetism," *The Journal of Physical Chemistry Letters*, vol. 15, pp. 1070–1078, 2024.

[61] H. Liu, J. Gao, and J. Zhao, "From boron cluster to two-dimensional boron sheet on cu (111) surface: growth mechanism and hole formation," *Scientific reports*, vol. 3, no. 1, p. 3238, 2013.

[62] Z. Guo, L. Zhang, T. Azam, and Z.-S. Wu, "Recent advances and key challenges of the emerging mbenes from synthesis to applications," *MetalMat*, p. e12, 2023.

[63] Z. Guo, J. Zhou, and Z. Sun, "New two-dimensional transition metal borides for li ion batteries and electrocatalysis," *Journal of Materials Chemistry A*, vol. 5, no. 45, pp. 23 530–23 535, 2017.

[64] A. Carlsson, J. Rosen, and M. Dahlqvist, "Theoretical predictions of phase stability for orthorhombic and hexagonal ternary mab phases," *Physical Chemistry Chemical Physics*, vol. 24, no. 18, pp. 11 249–11 258, 2022.

[65] G. Zhang, X. Li, K. Chen, Y. Guo, D. Ma, and K. Chu, "Tandem electrocatalytic nitrate reduction to ammonia on mbenes," *Angewandte Chemie International Edition*, vol. 62, no. 13, p. e202300054, 2023.

[66] J. Si, J. Yu, H. Lan, L. Niu, J. Luo, Y. Yu, L. Li, Y. Ding, M. Zeng, and L. Fu, "Chemical potential-modulated ultrahigh-phase-purity growth of ultrathin transition-metal boride single crystals," *Journal of the American Chemical Society*, vol. 145, no. 7, pp. 3994–4002, 2023.

[67] Y. Zhang, Z. Guo, Y. Fang, C. Tang, F. Meng, N. Miao, B. Sa, J. Zhou, and Z. Sun, "Rational design of bimetallic mbene for efficient electrocatalytic nitrogen reduction," *Journal of Colloid and Interface Science*, 2024.

[68] H. Sun, J. Meng, L. Jiao, F. Cheng, and J. Chen, "A review of transition-metal boride/phosphide-based materials for catalytic hydrogen generation from hydrolysis of boron-hydrides," *Inorganic Chemistry Frontiers*, vol. 5, no. 4, pp. 760–772, 2018.

[69] M. Ade and H. Hillebrecht, "Ternary borides cr2alb2, cr3alb4, and cr4alb6: The first members of the series (crb2) n cral with n= 1, 2, 3 and a unifying concept for ternary borides as mab-phases," *Inorganic chemistry*, vol. 54, no. 13, pp. 6122–6135, 2015.

[70] M. Dahlqvist, Q. Tao, J. Zhou, J. Palisaitis, P. O. Persson, and J. Rosen, "Theoretical prediction and synthesis of a family of atomic laminate metal borides with in-plane chemical ordering," *Journal of the American Chemical Society*, vol. 142, no. 43, pp. 18 583–18 591, 2020.

[71] T. Bo, P.-F. Liu, J. Zhang, F. Wang, and B.-T. Wang, "Tetragonal and trigonal mo 2 b 2 monolayers: two new low-dimensional materials for li-ion and na-ion batteries," *Physical Chemistry Chemical Physics*, vol. 21, no. 9, pp. 5178–5188, 2019.

[72] X. Gonze and C. Lee, "Dynamical matrices, born effective charges, dielectric permittivity tensors, and interatomic force constants from density-functional perturbation theory," *Physical Review B*, vol. 55, no. 16, p. 10355, 1997.

[73] R. Khaledialidusti, M. Khazaei, V. Wang, N. Miao, C. Si, J. Wang, and J. Wang, "Exploring structural, electronic, and mechanical properties of 2d hexagonal mbenes," *Journal of Physics: Condensed Matter*, vol. 33, no. 15, p. 155503, 2021.

[74] T. Bo, P.-F. Liu, J. Xu, J. Zhang, Y. Chen, O. Eriksson, F. Wang, and B.-T. Wang, "Hexagonal ti 2 b 2 monolayer: a promising anode material offering high rate capability for li-ion and na-ion batteries," *Physical Chemistry Chemical Physics*, vol. 20, no. 34, pp. 22 168–22 178, 2018.

[75] T. Hu, M. Wang, X. Wang, Y. Zhou, and C. Li, "Unraveling surface functionalization of cr2b2t2 (t= oh, o, cl, h) mbene by first-principles calculations," *Computational Materials Science*, vol. 199, p. 110810, 2021.

[76] Y. Gao, E. Wang, Y. Zheng, J. Zhou, and Z. Sun, "Hexagonal mbenes-supported single atom as electrocatalysts for the nitrogen reduction reaction," *Energy Material Advances*, vol. 4, p. 0039, 2023.

[77] G. Kucinskis, G. Bajars, and J. Kleperis, "Graphene in lithium ion battery cathode materials: A review," *Journal of Power Sources*, vol. 240, pp. 66–79, 2013.

[78] Y. Zhu and X. Wu, "Heterostructured materials," *Progress in Materials Science*, vol. 131, p. 101019, 2023.

[79] R. Sahu, D. Bogdanovski, J.-O. Achenbach, S. Zhang, M. Hans, D. Primetzhofer, J. M. Schneider, and C. Scheu, "Direct mob mbene domain formation in magnetron sputtered moalb thin films," *Nanoscale*, vol. 13, no. 43, pp. 18 077–18 083, 2021.

[80] P. Hou, J. Liu, D. Jin, Y. Tian, X. Liu, Y. Xie, F. Du, Y. Gogotsi, A. Vojvodic, and X. Meng, "P-type ohmic contacts of mbenes with mos2 for nanodevices and logic circuits," *2D Materials*, vol. 9, no. 4, p. 045022, 2022.

[81] P. Wang, F. Yin, M. ur Rahman, M. A. Khan, and D. Baleanu, "Unveiling complexity: Exploring chaos and solitons in modified nonlinear schrödinger equation," *Results in Physics*, vol. 56, p. 107268, 2024.

[82] F. A. Berezin and M. Shubin, *The Schrödinger Equation*. Springer Science & Business Media, 2012, vol. 66.

[83] E. Nelson, "Derivation of the schrödinger equation from newtonian mechanics," *Physical review*, vol. 150, no. 4, p. 1079, 1966.

[84] G. Fibich, *The nonlinear Schrödinger equation*. Springer, 2015, vol. 192.

[85] M. R. Fiechter and J. O. Richardson, "Understanding the cavity born-oppenheimer approximation," *arXiv preprint arXiv:2401.03532*, 2024.

[86] M. Born, "Born-oppenheimer approximation," *Ann. Phys*, vol. 84, pp. 457–484, 1927.

[87] M. Baer, S. H. Lin, A. Alijah, S. Adhikari, and G. D. Billing, "Extended approximated born-oppenheimer equation. i. theory," *Physical Review A*, vol. 62, no. 3, p. 032506, 2000.

[88] M. Sunder, "Born–oppenheimer approximation," *Jour. Chem. Phy*, vol. 6, pp. 201–209, 2000.

[89] C. D. Sherrill, "The born-oppenheimer approximation," *School of Chemistry and Biochemistry, Georgia Institute of Technology*, vol. 242, 2005.

[90] W. KOHN and J. A. POPLE, "Additional background material on the nobel prize in chemistry 1998."

[91] M. Orio, D. A. Pantazis, and F. Neese, "Density functional theory," *Photosynthesis research*, vol. 102, pp. 443–453, 2009.

[92] T. L. Gilbert, "Hohenberg-kohn theorem for nonlocal external potentials," *Physical Review B*, vol. 12, no. 6, p. 2111, 1975.

[93] M. Ernzerhof and G. E. Scuseria, "Perspective on "inhomogeneous electron gas" hohenberg p, kohn w (1964) phys rev 136: B864," *Theoretical Chemistry Accounts*, vol. 103, pp. 259–262, 2000.

[94] J. Riess and W. Münch, "The theorem of hohenberg and kohn for subdomains of a quantum system," *Theoretica chimica acta*, vol. 58, pp. 295–300, 1981.

[95] P. Hohenberg and W. Kohn, "Inhomogeneous electron gas," *Physical review*, vol. 136, no. 3B, p. B864, 1964.

[96] K. Ramachandran, D. Gopakumar, and K. Namboori, *Basis sets*. Springer, 2008.

[97] N. T. Maitra, A. Wasserman, and K. Burke, "What is time-dependent density functional theory? successes and challenges," in *Electron Correlations and Materials Properties 2*. Springer, 2003, pp. 285–298.

[98] U. Von Barth and L. Hedin, "A local exchange-correlation potential for the spin polarized case. i," *Journal of Physics C: Solid State Physics*, vol. 5, no. 13, p. 1629, 1972.

[99] F. A. Hamprecht, A. J. Cohen, D. J. Tozer, and N. C. Handy, "Development and assessment of new exchange-correlation functionals," *The Journal of chemical physics*, vol. 109, no. 15, pp. 6264–6271, 1998.

[100] J. Cioslowski and K. Pernal, "Local-density-matrix approximation: Exact asymptotic results for a high-density homogeneous electron gas," *Physical Review B*, vol. 71, no. 11, p. 113103, 2005.

[101] P. P. Rushton, "Towards a non-local density functiona description of exchange and correlation," Ph.D. dissertation, Durham University, 2002.

[102] D. M. Ceperley and B. J. Alder, "Ground state of the electron gas by a stochastic method," *Physical review letters*, vol. 45, no. 7, p. 566, 1980.

[103] G. A. DiLabio and A. Otero-de-la Roza, "Noncovalent interactions in density functional theory," *Reviews in computational chemistry*, vol. 29, pp. 1–97, 2016.

[104] O. Karalti, "Correcting density functional theory methods for dispersion interactions using pseudopotentials," Ph.D. dissertation, University of Pittsburgh, 2014.

[105] S. Grimme, J. Antony, S. Ehrlich, and H. Krieg, "A consistent and accurate ab initio parametrization of density functional dispersion correction (dft-d) for the 94 elements h-pu," *The Journal of chemical physics*, vol. 132, no. 15, 2010.

[106] S. Grimme, S. Ehrlich, and L. Goerigk, "Effect of the damping function in dispersion corrected density functional theory," *Journal of computational chemistry*, vol. 32, no. 7, pp. 1456–1465, 2011.

[107] S. Grimme, "Semiempirical gga-type density functional constructed with a long-range dispersion correction," *Journal of computational chemistry*, vol. 27, no. 15, pp. 1787–1799, 2006.

[108] ——, "Accurate description of van der waals complexes by density functional theory including empirical corrections," *Journal of computational chemistry*, vol. 25, no. 12, pp. 1463–1473, 2004.

[109] I. Y. Muhammad, "Structural and electronic properties of 2d chalcogenides," in *Journal of Physics: Conference Series*, vol. 1719, no. 1. IOP Publishing, 2021, p. 012029.

[110] W. Reckien, F. Janetzko, M. F. Peintinger, and T. Bredow, "Implementation of empirical dispersion corrections to density functional theory for periodic systems," *Journal of computational chemistry*, vol. 33, no. 25, pp. 2023–2031, 2012.

[111] E. Caldeweyher, S. Ehlert, A. Hansen, H. Neugebauer, S. Spicher, C. Bannwarth, and S. Grimme, "A generally applicable atomic-charge dependent london dispersion correction," *The Journal of chemical physics*, vol. 150, no. 15, 2019.

[112] J. Hermann, M. Stöhr, S. Góger, S. Chaudhuri, B. Aradi, R. J. Maurer, and A. Tkatchenko, "libmbd: A general-purpose package for scalable quantum many-body dispersion calculations," *The Journal of Chemical Physics*, vol. 159, no. 17, 2023.

[113] B. Amadon, "First-principles dft+ dmft calculations of structural properties of actinides: Role of hund's exchange, spin-orbit coupling, and crystal structure," *Physical Review B*, vol. 94, no. 11, p. 115148, 2016.

[114] N. E. Benti, G. S. Gurmesa, C. A. Geffe, A. M. Mohammed, G. A. Tiruye, and Y. S. Mekonnen, "Sodium-ion diffusion studies of the cathode–electrolyte interfaces (na x o 2@ na 2 co 3, x= 1 and 2) and discharge products of non-aqueous rechargeable sodium–air batteries," *Journal of Materials Chemistry A*, vol. 10, no. 15, pp. 8501–8514, 2022.

[115] V. I. Anisimov, F. Aryasetiawan, and A. Lichtenstein, "First-principles calculations of the electronic structure and spectra of strongly correlated systems: the lda+ u method," *Journal of Physics: Condensed Matter*, vol. 9, no. 4, p. 767, 1997.

[116] E. Morosan, D. Natelson, A. H. Nevidomskyy, and Q. Si, "Strongly correlated materials," *Advanced Materials*, vol. 24, no. 36, pp. 4896–4923, 2012.

[117] V. I. Anisimov, "Electronic structure of strongly correlated materials," in *AIP Conference Proceedings*, vol. 1297, no. 1. American Institute of Physics, 2010, pp. 3–134.

[118] B. Himmetoglu, A. Floris, S. De Gironcoli, and M. Cococcioni, "Hubbard-corrected dft energy functionals: The lda+ u description of correlated systems," *International Journal of Quantum Chemistry*, vol. 114, no. 1, pp. 14–49, 2014.

[119] X.-D. Wen, R. L. Martin, T. M. Henderson, and G. E. Scuseria, "Density functional theory studies of the electronic structure of solid state actinide oxides," *Chemical reviews*, vol. 113, no. 2, pp. 1063–1096, 2013.

[120] S. A. Trygubenko and D. J. Wales, "A doubly nudged elastic band method for finding transition states," *The Journal of chemical physics*, vol. 120, no. 5, pp. 2082–2094, 2004.

[121] Y. Elbaz, D. Furman, and M. Caspary Toroker, "Modeling diffusion in functional materials: From density functional theory to artificial intelligence," *Advanced Functional Materials*, vol. 30, no. 18, p. 1900778, 2020.

[122] H. JóNssoN, G. MILL, and K. W. JAcosEN, "Nuclged elastic band method for finding minimum en-ergy paths of transitions."

[123] H. P. Hratchian and H. B. Schlegel, "Finding minima, transition states, and following reaction pathways on ab initio potential energy surfaces," in *Theory and applications of computational chemistry*. Elsevier, 2005, pp. 195–249.

[124] P. Durand and J.-P. Malrieu, "Effective hamiltonians and pseudo-operators as tools for rigorous modelling," *Advances in Chemical Physics: Ab Initio Methods in Quantum Chemistry Part I*, vol. 67, pp. 321–412, 1987.

[125] S. V. Ramanujam, "Band structure of graphene using empirical pseudopotentials," Arizona State University, Tech. Rep., 2015.

[126] A. Kubaib, P. M. Imran, and A. A. Basha, "Applications of the vienna ab initio simulation package, dft and molecular interaction studies for investigating the electrochemical stability and solvation performance of non-aqueous namf6 electrolytes for sodium-ion batteries," *Computational and Theoretical Chemistry*, vol. 1217, p. 113934, 2022.

[127] C. Paduani, "Electronic structure of magnesium diboride and related compounds," *physica status solidi (b)*, vol. 240, no. 3, pp. 574–583, 2003.

[128] H. Kouarta, K. Zanat, and H. Belkhir, "Magnetic behavior of superconductor 2h-nbse 2 intercalated with iron: first principle study," *Journal of Superconductivity and Novel Magnetism*, vol. 32, pp. 805–819, 2019.

[129] H. J. Kulik and N. Marzari, "Transition-metal dioxides: A case for the intersite term in hubbard-model functionals," *The Journal of chemical physics*, vol. 134, no. 9, 2011.

[130] L. Xiong, J. Liu, X. Zhang, Q. Tao, and P. Zhu, "Radial x-ray diffraction study of the static strength and equation of state of mob2 to 85 gpa," *Journal of Alloys and Compounds*, vol. 623, pp. 442–446, 2015.

[131] Q. Tao, X. Zhao, Y. Chen, J. Li, Q. Li, Y. Ma, J. Li, T. Cui, P. Zhu, and X. Wang, "Enhanced vickers hardness by quasi-3d boron network in mob 2," *RSC advances*, vol. 3, no. 40, pp. 18 317–18 322, 2013.

[132] A. Jain, S. P. Ong, G. Hautier, W. Chen, W. D. Richards, S. Dacek, S. Cholia, D. Gunter, D. Skinner, G. Ceder, and K. a. Persson, "Commentary: The Materials Project: A materials genome approach to accelerating materials innovation," *APL Materials*, vol. 1, no. 1, p. 011002, 2013. [Online]. Available: https://doi.org/10.1063/1.4812323

[133] I. Shein, K. Shein, and A. Ivanovskii, "First-principles study on the structural, cohesive and electronic properties of rhombohedral mo2 b5 as compared with hexagonal mo b2," *Physica B, Condensed Matter*, vol. 387, pp. 184–189, 2007.

[134] M. Zhang, H. Wang, H. Wang, T. Cui, and Y. Ma, "Structural modifications and mechanical properties of molybdenum borides from first principles," *The Journal of Physical Chemistry C*, vol. 114, no. 14, pp. 6722–6725, 2010.

[135] L. Hui, Z. Xie, C. Li, and Z.-Q. Chen, "Fex (x= b, n) binary compounds: First-principles calculations of electronic structures, theoretic hardness and magnetic properties," *Journal of Magnetism and Magnetic Materials*, vol. 451, pp. 761–769, 2018.

[136] A. Ahmadi, M. Masoudi, N. Taghizade, H. Jafari, and M. Faghihnasiri, "Study of mechanical and electronic properties of single-layer feb2," *Physica E: Low-dimensional Systems and Nanostructures*, vol. 112, pp. 71–77, 2019.

[137] L. Voroshnin, L. Lyakhovich, G. Panich, and G. Protasevich, "The structure of fe-b alloys," *Metal Science and Heat Treatment*, vol. 1970, pp. 732–735, 1970.

[138] Y. Zhang, Y.-W. Tan, H. L. Stormer, and P. Kim, "Experimental observation of the quantum hall effect and berry's phase in graphene," *nature*, vol. 438, no. 7065, pp. 201–204, 2005.

[139] W. Yu, L. Sisi, Y. Haiyan, and L. Jie, "Progress in the functional modification of graphene/graphene oxide: A review," *RSC advances*, vol. 10, no. 26, pp. 15 328–15 345, 2020.

[140] R. E. Johnsen and P. Norby, "Capillary-based micro-battery cell for in situ x-ray powder diffraction studies of working batteries: a study of the initial intercalation and deintercalation of lithium into graphite," *Journal of Applied Crystallography*, vol. 46, pp. 1537–1543, 2013.

[141] P. Gamlen and J. White, "Structure and dynamics of microcrystalline graphite, graphon, by neutron scattering," *Journal of the Chemical Society. Faraday Transactions 2.*, vol. 72, pp. 446–455, 1976.

[142] A. Majed, M. Torkamanzadeh, C. F. Nwaokorie, K. Eisawi, C. Dun, A. Buck, J. J. Urban, M. M. Montemore, V. Presser, and M. Naguib, "Toward mbenes battery electrode materials: Layered molybdenum borides for li-ion batteries," *Small Methods*, p. 2300193, 2023.

[143] Y. Chen, Y. Liang, C. Zhou, Z. Li, D. Wu, J. Li, P. Dong, Y. Zhang, X. Tian, and X. Shi, "Heterogeneous-structured molybdenum diboride as a novel and promising anode for lithium-ion batteries," *Small*, p. 2311782, 2024.

[144] G. Barik and S. Pal, "Monolayer molybdenum diborides containing flat and buckled boride layers as anode materials for lithium-ion batteries," *Physical Chemistry Chemical Physics*, 2023.

[145] J. Zhu, R. Duan, S. Zhang, N. Jiang, Y. Zhang, and J. Zhu, "The application of graphene in lithium ion battery electrode materials," *SpringerPlus*, vol. 3, pp. 1–8, 2014.

[146] Y. Wu, D. B. Farmer, F. Xia, and P. Avouris, "Graphene electronics: Materials, devices, and circuits," *Proceedings of the IEEE*, vol. 101, no. 7, pp. 1620–1637, 2013.

[147] A. Massaro, A. Pecoraro, A. B. Munoz-Garcia, and M. Pavone, "First-principles study of na intercalation and diffusion mechanisms at 2d mos2/graphene interfaces," *The Journal of Physical Chemistry C*, vol. 125, no. 4, pp. 2276–2286, 2021.

[148] J. Li, Q. Peng, J. Zhou, and Z. Sun, "Mos2/ti2ct2 (t= f, o) heterostructures as promising flexible anodes for lithium/sodium ion batteries," *The Journal of Physical Chemistry C*, vol. 123, no. 18, pp. 11 493–11 499, 2019.

[149] S. Ali, X. Zhang, M. S. Javed, H. U. Shah, A. Ahmad, M. D. Albaqami, M. Sheikh, A. M. Hassan, X. Wei, J. Wang *et al.*, "Mos2/ti3co2 heterostructure-based ceramics as promising electrode material for high-performance monovalent energy storage devices," *Ceramics International*, vol. 50, no. 3, pp. 4782–4789, 2024.

[150] N. Li, Y. Li, X. Zhu, C. Huang, and J. Fan, "Theoretical investigation of the intercalation mechanism of vs2/mxene heterostructures as anode materials for metal-ion batteries," *Applied Surface Science*, vol. 543, p. 148772, 2021.